Title

Sleep Regulation by Neurotensinergic Neurons in a Thalamo-Amygdala Circuit

Journal

Neuron, 103(2)

ISSN

0896-6273

Authors

Ma, Chenyan
Zhong, Peng
Liu, Danqian
et al.

Publication Date

2019-07-01

DOI

10.1016/j.neuron.2019.05.015

Peer reviewed

Article

Neuron

Sleep Regulation by Neurotensinergic Neurons in a Thalamo-Amygdala Circuit

Graphical Abstract

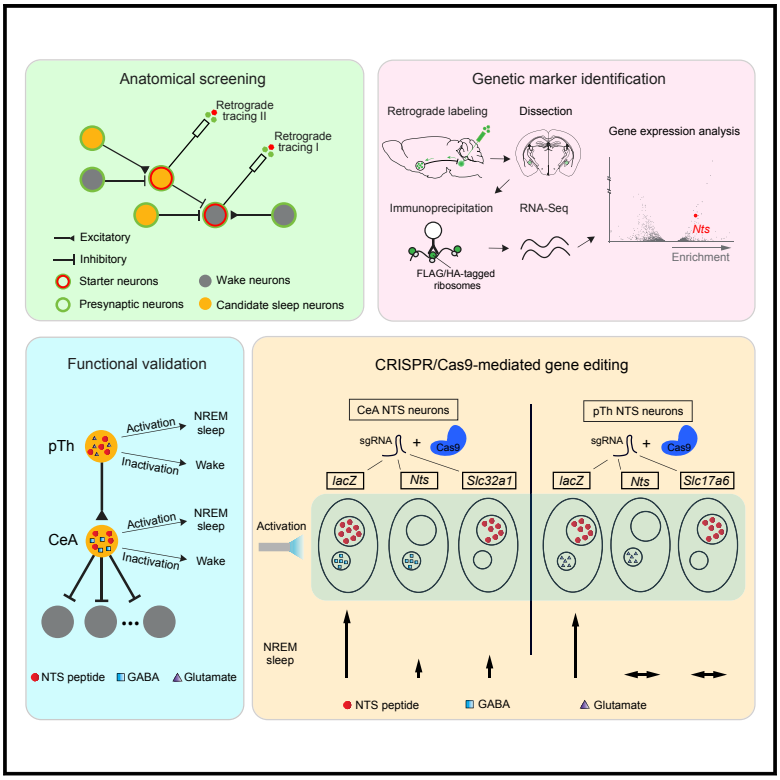

Highlights

- A three-step approach was used for whole-brain screening for sleep-promoting neurons
- NTS-positive GABAergic CeA neurons widely inhibit wake neurons and promote NREM sleep
- NTS-positive glutamatergic pTh neurons excite CeA NTS neurons and promote NREM sleep
- CeA and pTh neurons require both NTS and GABA and glutamate transmission to promote sleep

Authors

Chenyan Ma, Peng Zhong, Danqian Liu, ..., Wei-Cheng Chang, Brian Kim, Yang Dan

Correspondence

ydan@berkeley.edu

In Brief

Using a three-step approach for systematic screening, Ma et al. identified GABAergic neurons in CeA and glutamatergic neurons in the posterior thalamus that promote NREM sleep. Each population uses both the NTS peptide and a classical neurotransmitter to promote sleep.

Ma et al., 2019, Neuron *103*, 1–12
July 17, 2019
https://doi.org/10.1016/j.neuron.2019.05.015

CellPress

Please cite this article in press as: Ma et al., Sleep Regulation by Neurotensinergic Neurons in a Thalamo-Amygdala Circuit, Neuron (2019), https://doi.org/10.1016/j.neuron.2019.05.015

Neuron
Article

Sleep Regulation by Neurotensinergic Neurons in a Thalamo-Amygdala Circuit

Chenyan Ma,[1] Peng Zhong,[1] Danqian Liu,[1] Zeke Katsh Barger,[1] Li Zhou,[2] Wei-Cheng Chang,[1] Brian Kim,[1] and Yang Dan[1,3,*]

[1]Division of Neurobiology, Department of Molecular and Cell Biology, Helen Wills Neuroscience Institute, Howard Hughes Medical Institute, University of California, Berkeley, Berkeley, CA 94720, USA

[2]Eli and Edythe Broad Center of Regeneration Medicine and Stem Cell Research, Department of Neurology, University of California, San Francisco, San Francisco, CA 94143, USA

[3]Lead Contact

*Correspondence: ydan@berkeley.edu

https://doi.org/10.1016/j.neuron.2019.05.015

SUMMARY

A crucial step in understanding the sleep-control mechanism is to identify sleep neurons. Through systematic anatomical screening followed by functional testing, we identified two sleep-promoting neuronal populations along a thalamo-amygdala pathway, both expressing neurotensin (NTS). Rabies-mediated monosynaptic retrograde tracing identified the central nucleus of amygdala (CeA) as a major source of GABAergic inputs to multiple wake-promoting populations; gene profiling revealed NTS as a prominent marker for these CeA neurons. Optogenetic activation and inactivation of NTS-expressing CeA neurons promoted and suppressed non-REM (NREM) sleep, respectively, and optrode recording showed they are sleep active. Further tracing showed that CeA GABAergic NTS neurons are innervated by glutamatergic NTS neurons in a posterior thalamic region, which also promote NREM sleep. CRISPR/Cas9-mediated NTS knockdown in either the thalamic or CeA neurons greatly reduced their sleep-promoting effect. These results reveal a novel thalamo-amygdala circuit for sleep generation in which NTS signaling is essential for both the upstream glutamatergic and downstream GABAergic neurons.

INTRODUCTION

A well-studied brain region for sleep generation is the preoptic area of the anterior hypothalamus (Nauta, 1946; Von Economo, 1930) in which a subset of GABAergic neurons promotes sleep by inhibiting wake-promoting neuronal populations (Chung et al., 2017; Lu et al., 2000; Sallanon et al., 1989; Sherin et al., 1998; Steininger et al., 2001; Zhang et al., 2015). In addition to the preoptic area, recent studies have identified sleep-promoting neurons in posterior parts of the hypothalamus (Jego et al., 2013; Konadhode et al., 2013; Liu et al., 2017; Tsunematsu et al., 2014), the parafacial zone in the medulla (Anaclet et al., 2014), the basal ganglia (Oishi et al., 2017; Yuan et al., 2017), the ventral tegmental area (VTA) (Yang et al., 2018; Yu et al., 2019), and the ventrolateral periaqueductal gray (Weber et al., 2015). This indicates that the sleep-control network is widely distributed, spanning multiple anatomical locations. Given the diversity of brain regions involved, however, it is unclear how many additional sleep-promoting neurons remain to be discovered and whether there is any organizational logic of the sleep-control network. To address these questions, we employed a three-step approach for systematic identification of sleep-promoting neurons consisting of anatomical screening, marker identification, and functional validation.

In principle, a neuron could promote sleep by either inhibiting wake-promoting neurons (Brown et al., 2012; Saper et al., 2010; Scammell et al., 2017; Weber and Dan, 2016) or exciting other sleep-promoting neurons. Based on this simple logic, we designed a strategy for whole-brain screening for candidate sleep neurons. Using rabies virus (RV)-mediated transsynaptic tracing, we first identified GABAergic neurons that broadly inhibit multiple wake-promoting neuronal populations. To gain genetic access to these candidate sleep neurons, we identified their molecular markers using gene-expression profiling. The role of these neurons in sleep regulation was then tested using bidirectional optogenetic manipulation. Once functionally validated, the GABAergic sleep neurons were targeted for further RV tracing, and their glutamatergic inputs were tested as additional candidate sleep neurons.

This sequential screening approach led to the identification of two neuronal populations along a thalamo-amygdala pathway that promote non-REM (NREM) sleep. Interestingly, both the GABAergic and glutamatergic populations express the peptide neurotensin (NTS). CRISPR/Cas9-mediated knockdown of either NTS or the vesicular transporter for GABA and glutamate strongly reduced the sleep-promoting effect of each population, indicating that these neurons promote NREM sleep using both classical transmitters and the neuropeptide NTS.

RESULTS

Detection of Candidate Sleep Neurons in the Central Nucleus of Amygdala

To identify candidate sleep neurons that inhibit wake-promoting neurons, we performed RV-mediated transsynaptic tracing from seven wake-promoting populations, including

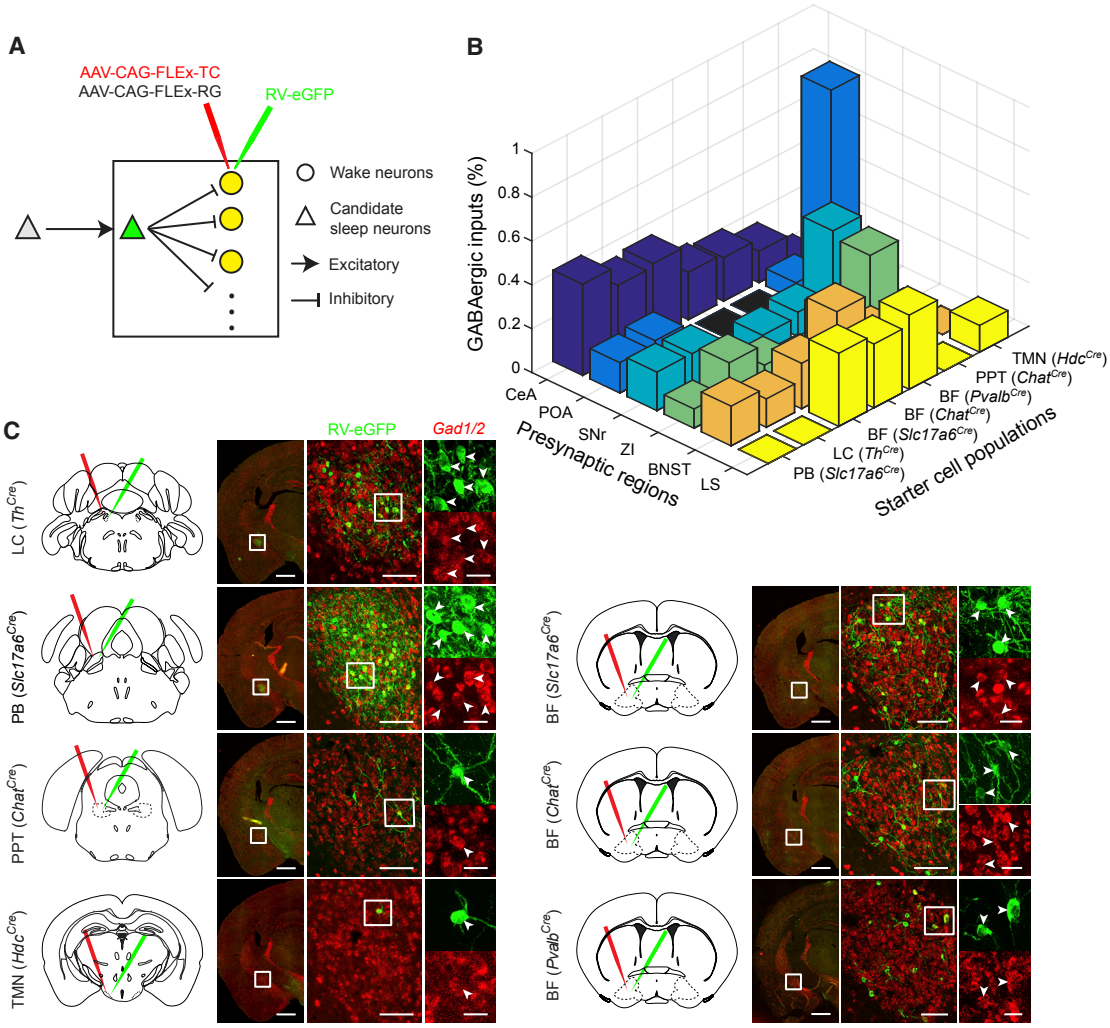

Figure 1. Detection of Candidate Sleep Neurons in the CeA through Anatomical Screening

(A) Schematic for identifying candidate sleep neurons that inhibit multiple wake-promoting populations using RV-mediated retrograde tracing.

(B) Percentage of RV-labeled GABAergic neurons in each presynaptic region for each targeted wake-promoting population. Included are presynaptic regions with >5 RV-labeled cells for at least 3 of the targeted wake populations. Presynaptic regions too close to the starter cell population are excluded from the analysis due to potential local contamination (Beier et al., 2015; Weissbourd et al., 2014) (e.g., preoptic area [POA] for basal forebrain [BF] targeting), indicated by black. BNST, bed nucleus of the stria terminalis; LS, lateral septum; SNr, substantia nigra pars reticulata; ZI, zona incerta.

(C) CeA GABAergic neurons innervate multiple wake-promoting populations. Left: coronal diagrams showing virus injection sites and Cre lines used for RV tracing. Right: fluorescence images of RV-labeled presynaptic neurons in CeA with progressively higher magnification (white box in each image shows the region enlarged in the next image on the right). Arrowheads indicate overlap between RV-EGFP (green) and *Gad1/2* (red). Scale bars represent 800 μm (left), 100 μm (middle), or 25 μm (right). BF, basal forebrain; PPT, pedunculopontine tegmentum; TMN, tuberomammillary nucleus.

See also Figure S1.

noradrenergic, histaminergic, cholinergic, glutamatergic, and GABAergic neurons distributed in the brainstem, hypothalamus, and basal forebrain (Brown et al., 2012; Saper et al., 2010; Scammell et al., 2017; Weber and Dan, 2016). An avian retroviral receptor (TVA) fused with mCherry (TC) and a rabies glycoprotein (RG) was expressed in each population by injecting two Cre-inducible adeno-associated virus (AAV) vectors (AAV2-CAG-FLEx-TC and AAV2-CAG-FLEx-RG) into the target region of the corresponding Cre mice (Figure 1A). A modified RV expressing EGFP (RV*dG*-EGFP+EnvA) was injected 3 weeks later to infect the TC-expressing target neurons (Figure S1) and label their presynaptic inputs (Weissbourd et al., 2014; Wickersham et al., 2007).

Fluorescence in situ hybridization (FISH) combined with immunohistochemistry (IHC) of *Gad1/2* (glutamate decarboxylase 1 or 2) and RV-EGFP revealed several brain regions with broad GABAergic innervation of the wake-promoting populations (Figure 1B), including the preoptic hypothalamus and zona incerta, both of which contain GABAergic sleep-promoting neurons (Chung et al., 2017; Liu et al., 2017; Lu et al., 2000; Sherin et al., 1998; Steininger et al., 2001; Zhang et al., 2015). Surprisingly, however, the most prominent source of GABAergic inputs

was found in a posterior part of the central nucleus of amygdala (CeA), especially its lateral subdivision (CeL) (Figure 1C). In fact, in addition to the wake-promoting populations targeted here, the CeA also innervates serotonergic neurons in the dorsal raphe (Weissbourd et al., 2014) and dopaminergic neurons in the VTA (Beier et al., 2015; Eban-Rothschild et al., 2016). Such broad GABAergic innervation of wake-promoting populations points to CeA neurons as strong candidates for sleep-promoting neurons.

NTS Is a Marker for CeA Candidate Sleep Neurons

The CeA is known to contain multiple subtypes of GABAergic neurons with distinct molecular markers, projection targets, and functional properties (Cai et al., 2014; Carter et al., 2013; Ciocchi et al., 2010; Douglass et al., 2017; Fadok et al., 2017; Haubensak et al., 2010; Janak and Tye, 2015; Kim et al., 2017; Li et al., 2013; McCall et al., 2015; Viviani et al., 2011; Zelikowsky et al., 2018). To identify molecular markers for the neurons projecting to the wake-promoting populations, we performed gene profiling using translating ribosome affinity purification (TRAP) (Ekstrand et al., 2014; Heiman et al., 2008). Cre-inducible herpes simplex virus (HSV) expressing the large ribosomal subunit protein Rpl10a fused with a FLAG and hemagglutinin (HA) tag (HSV-hEF1α-LSL-FlagHA-L10a) was injected into the locus coeruleus (LC) and parabrachial nucleus (PB) of *Gad2*^{Cre} mice. After 30–45 days of expression, the CeA was dissected, and the translating mRNA was isolated by immunoprecipitating (IP) the L10a protein from tissue lysate (Figure 2A).

RNA sequencing (RNA-seq) revealed multiple genes significantly enriched in immunoprecipitated RNAs from the LC- and PB-projecting CeA GABAergic neurons relative to the input RNAs (whole CeA lysates before immunoprecipitation; Figure 2B). In particular, we focused on the genes encoding neuropeptides, which are known to play important roles in behavioral regulation and serve as useful markers for cell types (Paul et al., 2017). We found three highly enriched neuropeptides, tachykinin 2 (TAC2), NTS, and prodynorphin (PDYN), all of which are strongly expressed in the CeA, but not in the nearby basolateral amygdala. In contrast, none of the highly enriched non-peptide markers (Figure 2B) exhibit restricted expression in the CeA (based on in situ hybridization data from the Allen Mouse Brain Atlas, Allen Institute for Brain Science: https://mouse.brain-map.org/). Double FISH in the posterior CeA showed a near-complete overlap between TAC2 and NTS and a strong overlap between PDYN and NTS (Kim et al., 2017) (Figure 2C). The majority of RV-labeled CeA neurons projecting to the LC, PB, or VTA expressed NTS (Figure 2D), but very few expressed PKCδ or enkephalin (Figure 2E), even though they are also prominent markers in the CeA (Haubensak et al., 2010; Kim et al., 2017). This is consistent with the gene profiling experiment showing that PKCδ and enkephalin are not enriched in the LC- and PB-projecting neurons relative to the input RNAs (Figure 2B). These results point to NTS as an effective marker for the candidate sleep neurons, allowing specific targeting of these cells using a knockin *Nts*^{Cre} mouse line (Leinninger et al., 2011) (Figure S2A). Whole-cell recordings in acute brain slices confirmed GABAergic innervation of several wake-promoting cell types by CeA NTS neurons (Figures S2B–S2E).

CeA NTS Neurons Are NREM Promoting and NREM Active

To test the causal role of the CeA NTS neurons in sleep generation, we injected Cre-inducible AAV expressing ChR2 fused with enhanced yellow fluorescent protein (ChR2-EYFP) into the posterior CeA of *Nts*^{Cre} mice. Laser stimulation (10 Hz, 120 s per trial) was applied randomly every 7–16 min in freely moving mice, and wake, REM, and NREM sleep was classified based on electroencephalogram (EEG) and electromyogram (EMG) recordings. Activation of CeA NTS neurons during the light phase caused a marked increase in NREM sleep and decrease in wakefulness (Figures 3A and 3B), and the EEG power spectrum during the laser-induced NREM state was indistinguishable from that during spontaneous NREM sleep outside of laser stimulation (Figure S3A). Immunohistochemical staining of Fos showed that the magnitude of increase in NREM sleep depends strongly on the number of CeA neurons activated by the laser (Figure S3B). To determine whether the increased NREM sleep was due to its increased initiation or maintenance, we analyzed the probability of transitions between each pair of brain states (Chung et al., 2017). NTS neuron activation significantly increased wake→NREM and NREM→NREM transitions while decreasing wake→wake, NREM→wake, and NREM→REM transitions (Figure 3C), indicating enhancement of both the initiation and maintenance of NREM sleep. Furthermore, optogenetic activation of NTS neurons during the dark phase also increased NREM sleep (Figures S3C; $p < 0.0001$, bootstrap), although the magnitude of the increase was smaller than that during the light phase ($p = 0.01$).

In contrast to ChR2-mediated activation, optogenetic silencing of CeA NTS neurons through the light-activated chloride channel iC++ significantly decreased NREM sleep and increased wakefulness (Figures 3D and 3E). These changes were caused by a decreased NREM→NREM transition and increased NREM→wake and NREM→REM transitions (Figure 3F). In control mice expressing EYFP without ChR2 or iC++, laser stimulation had no effect (Figures S3D and S3E), and the laser-induced changes in sleep and wakefulness were significantly different between ChR2 and control mice ($p < 0.01$, bootstrap) and between iC++ and control mice ($p < 0.01$). Together, these activation and inactivation experiments demonstrate the sleep-promoting function of CeA NTS neurons.

In addition to bidirectional manipulation, we also measured the endogenous sleep-wake activity of ChR2-tagged CeA NTS neurons using optrode recording (Anikeeva et al., 2011; Xu et al., 2015). High-frequency laser pulses (15 or 30 Hz, 5 or 10 ms per pulse, 16 pulses per train) were applied intermittently, and single units exhibiting reliable laser-evoked spiking at short latencies and low jitter were identified as NTS neurons (Figures 4A and 4B). To quantify the relative firing rates of each neuron in different brain states, we plotted its NREM-wake modulation $((R_{NREM} - R_{wake})/(R_{NREM} + R_{wake})$, where R is the mean firing rate within each state) versus REM-wake modulation $((R_{REM} - R_{wake})/(R_{REM} + R_{wake}))$. Of the 23 identified NTS neurons, the great majority fell in the upper right quadrant (Figure 4C), indicating that they are more active during NREM and

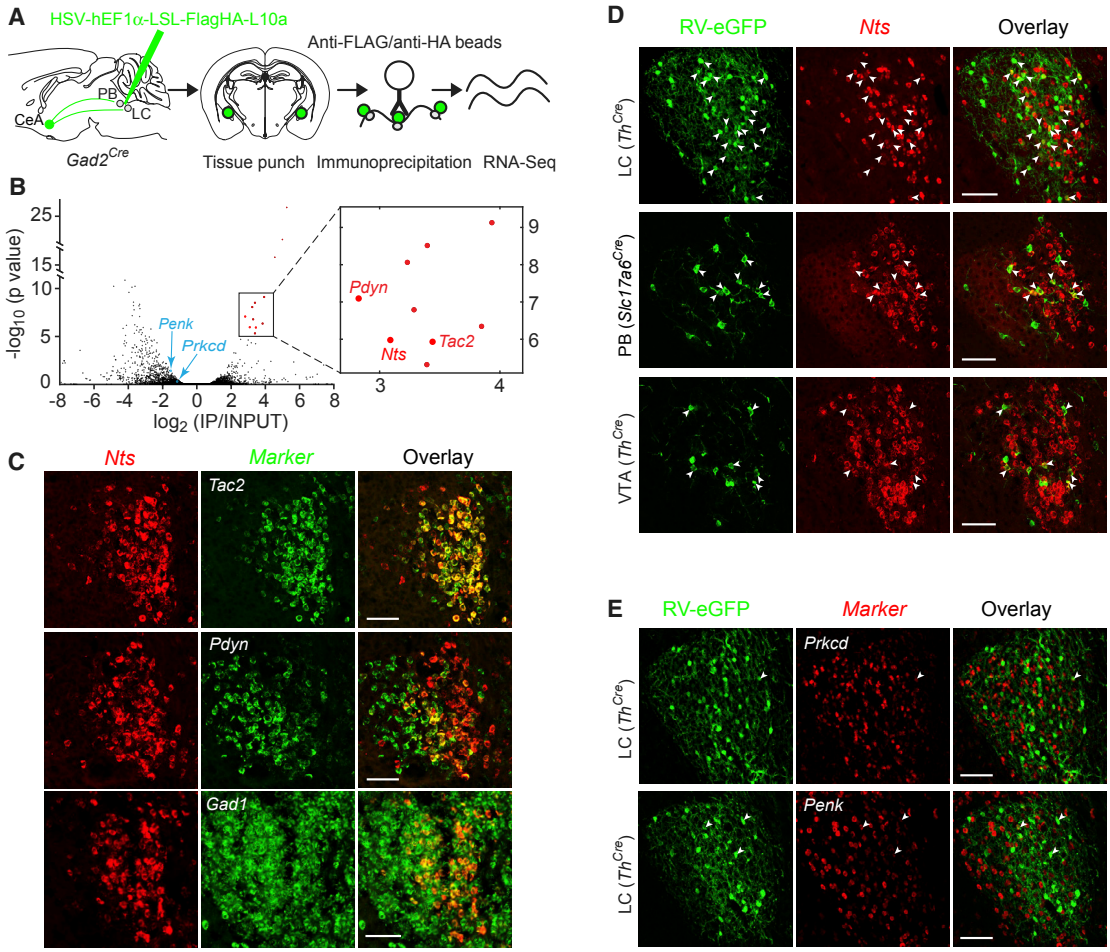

Figure 2. NTS Is a Marker for CeA Candidate Sleep Neurons

(A) Schematic of translating ribosome affinity purification (TRAP) for gene-expression profiling.

(B) TRAP sequencing result for LC- and PB-projecting CeA GABAergic neurons, with statistical significance plotted against fold enrichment in IP versus input fraction. CeA tissues from 4–5 mice were pooled in each of the two experimental replicates. The highly enriched genes (indicated in red) include *Rpl10a* (overexpressed by HSV, serving as a positive control for the gene profiling experiment), *Bcar1*, *Nedd9*, *Efs*, *Gtf2i*, *Arhgap36*, *NFatc2*, *Scyl2*, and *Ogt* in addition to the three peptides (*Nts*, *Tac2*, and *Pdyn*).

(C) Overlap between *Nts* and *Tac2* (91% of *Nts* and 86% of *Tac2*), *Nts* and *Pdyn* (76% of *Nts* and 54% of *Pdyn*), and *Nts* and *Gad1* (100% of *Nts*) in the posterior CeA based on double FISH. Scale bars, 100 μm.

(D) Overlap between RV-EGFP and *Nts* in posterior CeA, for retrograde tracing from LC (59.2% ± 1.6% of EGFP neurons express NTS, n = 3 mice), PB (67.2% ± 2.6%, n = 3 mice), and VTA (61.6% ± 2.8%, n = 3 mice). Scale bars, 100 μm.

(E) Overlap between RV-EGFP and PKCδ (8.6% ± 1.2%, n = 3 mice) or enkephalin (PENK, 9.1% ± 0.9%, n = 3 mice) for retrograde tracing from LC, which is significantly lower than the overlap with NTS (p = 0.001, t test). Scale bars, 100 μm.

See also Figure S2.

REM sleep than wakefulness (p = 0.04 for both NREM-wake and REM-wake modulation, t test). Individually, 9 neurons showed significantly higher rates during NREM sleep than wakefulness (p < 0.01, Wilcoxon rank sum test), and only 2 were more active during wakefulness; 13 neurons showed significantly higher firing rates during REM sleep than wakefulness, and only 1 showed the opposite. In contrast, the unidentified CeA neurons (n = 29) showed a much higher degree of functional diversity, including many neurons that were more active during wakefulness than sleep (Figure 4C, gray symbols). Thus, the NTS subpopulation of CeA neurons are sleep active as well as sleep promoting.

Identification of Glutamatergic Sleep Neurons in Posterior Thalamus

Having established that CeA NTS neurons are GABAergic sleep-promoting neurons, we next set out to identify their glutamatergic inputs; in principle, these upstream neurons could promote NREM sleep by exciting CeA neurons, thus serving as additional candidate sleep neurons (Figure 5A). RV-mediated retrograde tracing from CeA NTS neurons followed by FISH-IHC of *Slc17a6* (encoding VGLUT2) and RV-EGFP revealed two regions with strong glutamatergic inputs: the paraventricular nucleus of the thalamus (PVT) (Figures S4A and S4B) (Penzo et al., 2015; Ren et al., 2018; Zhu et al., 2018) and a posterior region of the

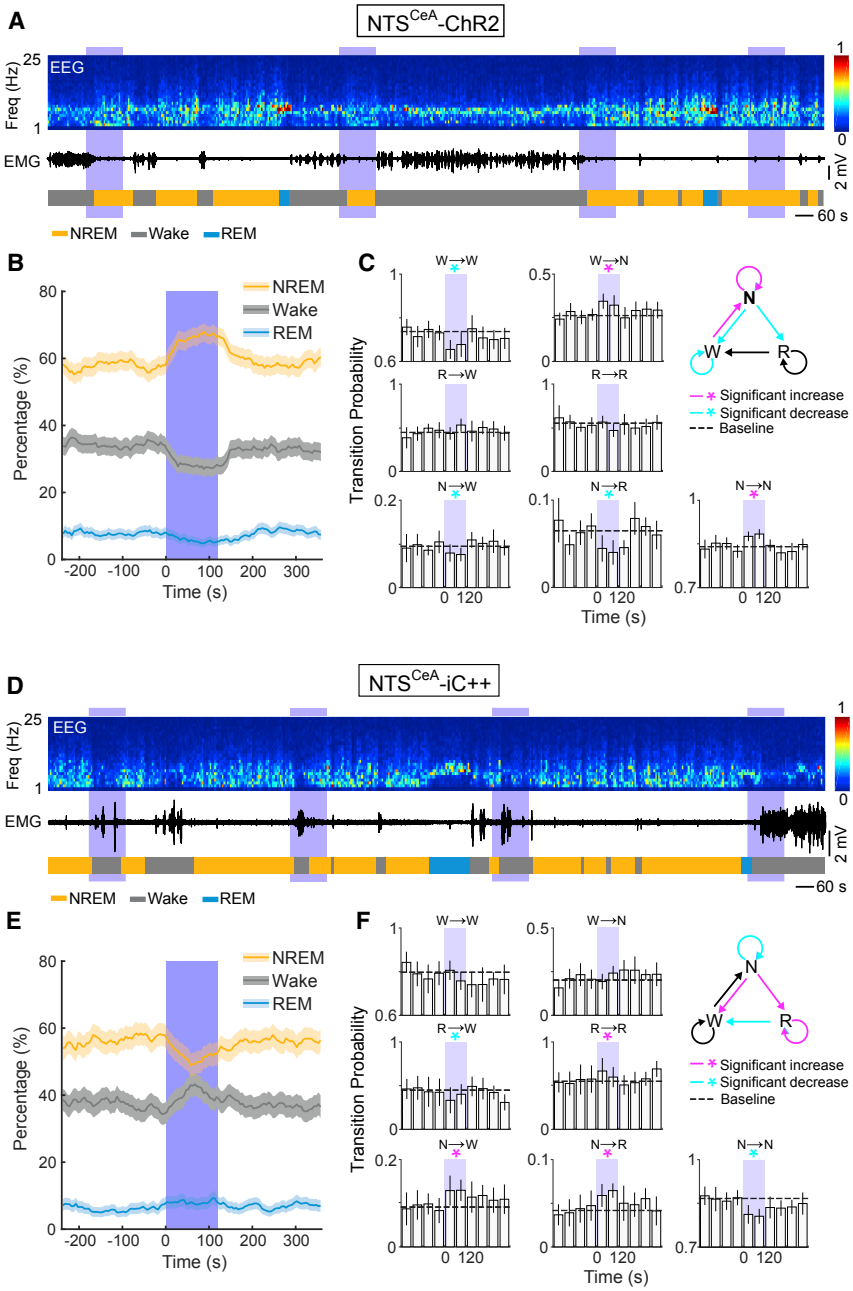

Figure 3. Optogenetic Activation and Inactivation of CeA NTS Neurons Enhances and Suppresses NREM Sleep, Respectively

(A) An example optogenetic activation experiment in a *Nts*^{Cre} mouse with AAV-EF1α-DIO-hChR2-EYFP injected into the posterior CeA. Shown are the EEG spectrogram, EMG trace, and brain states (color coded). Blue shading represents laser stimulation (10 Hz, 120 s). Freq., frequency.

(B) Percentage of time in NREM, REM, or the wake state before, during, and after laser stimulation, averaged from 12 mice. Laser stimulation significantly increased NREM sleep ($p < 0.0001$, bootstrap) and decreased wakefulness ($p < 0.0001$) and REM sleep ($p < 0.001$). Shading represents the 95% confidence interval (CI; bootstrap), and the blue stripe indicates the laser stimulation period.

(C) Effect of laser stimulation on transition probability between each pair of brain states. Each bar represents transition probability within each 20-s period (averaged across 3 consecutive 20-s bins within each 60 s). Error bar represents the 95% CI. Dashed line represents the baseline transition probability. N, NREM; R, REM; W, wake. W→R and R→N transitions are omitted, because they were rarely detected with or without laser stimulation. Magenta and cyan asterisk (*) indicates significant increase and decrease in transition probability during laser stimulation compared to baseline ($p < 0.05$, bootstrap). The diagram summarizes transitions that are significantly increased (magenta), decreased (cyan), or unaffected (black) by laser stimulation.

(D–F) Similar to (A)–(C), but for iC++-mediated optogenetic inactivation of NTS neurons (constant light, 120 s) in the posterior CeA ($p < 0.0001$ for a decrease in NREM and $p < 0.01$ and 0.001 for increases in REM and wake, n = 7 mice). (D) Similar to (A), (E) similar to (B), and (F) similar to (C).

See also Figure S3.

thalamus (Figures 5B, 5C, and 5F). Interestingly, in both regions, a large fraction of RV-labeled neurons also expressed NTS (Figures 5D–5F, S4C, and S4D).

To test the roles of these thalamic NTS neurons in sleep regulation, we applied bidirectional optogenetic manipulation. In the posterior region of the thalamus (herein referred to as "posterior thalamus," pTh), ChR2-mediated activation of NTS neurons caused a significant increase in NREM sleep and decrease in wakefulness (Figures 5G, S5A, and S5B), whereas iC++-mediated inactivation of these neurons had the opposite effects (Figures 5H and S5C). In contrast, activation of PVT NTS neurons did not promote sleep (Figure S4E) (Ren et al., 2018). Thus, among the glutamatergic candidate sleep neurons innervating CeA neurons, the NTS population in the posterior thalamus is confirmed as NREM-promoting neurons. To assess whether the NTS neurons in the posterior thalamus are naturally active during sleep, we performed double FISH of *Nts* and the activity marker gene *Fos*. Compared to control mice with undisturbed sleep-wake behavior, rebound sleep (RS) following deprivation strongly increased Fos expression in NTS neurons (Figure S5D), indicating that they are sleep active. Interestingly, Fos expression following sleep deprivation (SD) was also higher than the control though lower than following RS, suggesting that posterior thalamic NTS neurons are activated by sleep pressure in addition to sleep.

Both NTS Peptide and Classical Transmitters Contribute to NREM Sleep

The fact that both the CeA GABAergic and posterior thalamic glutamatergic NREM-promoting neurons express NTS raises

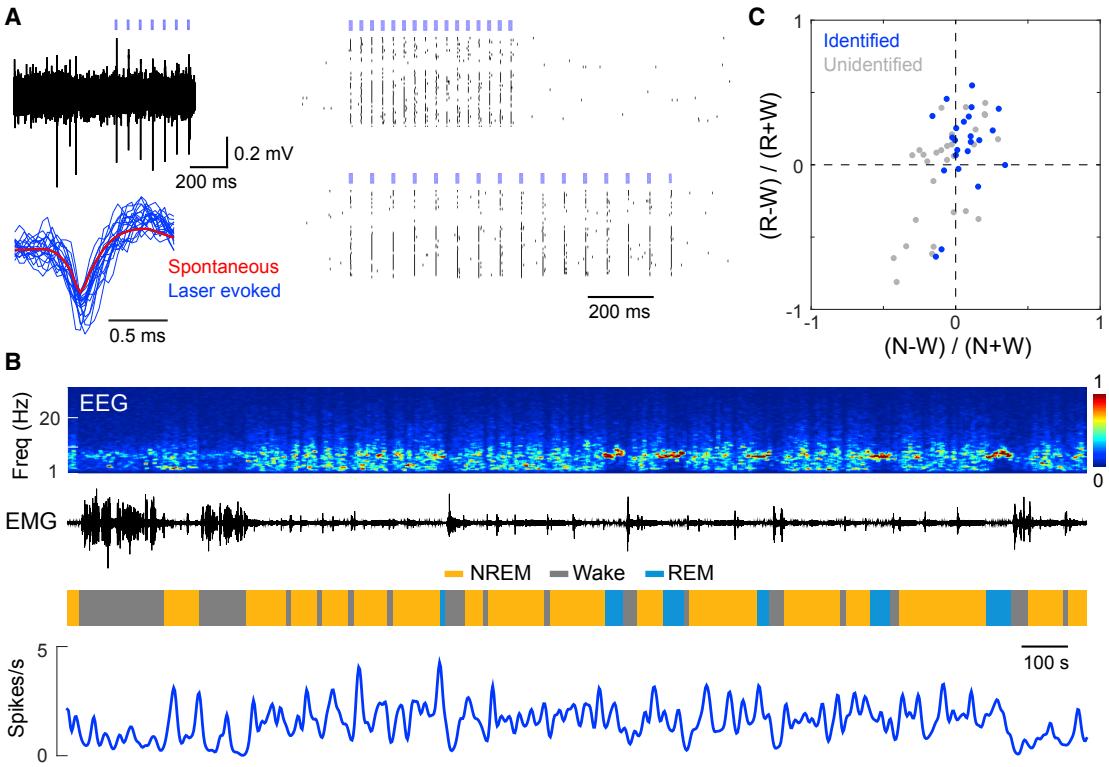

Figure 4. CeA NTS Neurons Are Preferentially Active during Sleep

(A) Example recording of spontaneous and laser-evoked spikes from an identified NTS neuron. Top left: raw trace. Blue ticks indicate laser pulses. Bottom left: comparison between laser-evoked (blue) and averaged spontaneous (red) spike waveforms. Right: spike raster showing multiple laser-stimulation trials at 15 and 30 Hz.

(B) Firing rate of the neuron together with the EEG spectrogram, EMG trace, and brain states (color coded). Freq., frequency.

(C) Firing rate modulation of all identified NTS (blue, n = 23) and unidentified (gray, n = 29) neurons in the CeA.

the possibility that the peptide itself plays a role in NREM sleep generation. To test this possibility, we used CRISPR/Cas9-mediated genome editing to knock down NTS expression in each population. In Nts^{Cre} mice crossed with Cre-inducible Cas9 knockin mice (Platt et al., 2014), we injected an AAV vector encoding both *Nts*-targeting single guide RNA (sgRNA) and Cre-inducible ChR2-mCherry into the CeA to express ChR2 in NTS-knockdown cells (Figure 6A). Compared to the control sgRNA targeting *lacZ*, *Nts*-targeting sgRNA caused an ~80% reduction of NTS expression in the infected neurons (Figures 6B and S6A). Optogenetic experiments showed that NTS knockdown greatly reduced the magnitude of NREM increase induced by ChR2-mediated activation of CeA NTS neurons (Figures 6C and 6D). This reduction was not due to a decreased firing of these neurons evoked by ChR2 activation (Figures S6B and S6C), indicating that the NTS peptide contributes significantly to the promotion of NREM sleep. We next performed CRISPR/Cas9-mediated knockdown of the vesicular GABA transporter (VGAT; encoded by *Slc32a1*) (Figures 6A and S6E), which plays a crucial role in GABAergic synaptic transmission (Kim and Kerschensteiner, 2017; Rau and Hentges, 2017). This also greatly reduced the NREM increase induced by optogenetic activation (Figures 6C and 6D), indicating that both GABA and NTS signaling are important for sleep regulation by CeA NTS neurons. In addition to the NREM increase induced by optogenetic activation, NTS and VGAT knockdown also caused small but significant reductions of baseline NREM sleep (Figures S7A and S7B).

We then tested the role of NTS signaling in posterior thalamic glutamatergic neurons using CRISPR/Cas9-mediated knockdown (Figures 7A, 7B, and S6D). Compared to the control *lacZ*-targeting sgRNA, *Nts*-targeting sgRNA largely eliminated the NREM increase induced by optogenetic activation of posterior thalamic NTS neurons (Figures 7C and 7D) in addition to reducing baseline sleep (Figures S7C). Similar effects were observed with the knockdown of VGLUT2 (Figures 7C, 7D, S6F, and S7D), which is crucial for glutamatergic synaptic transmission (Schweizer et al., 2014; Shen et al., 2018). These results indicate that sleep regulation by thalamic NTS neurons also depends on both the classical transmitter and the NTS neuropeptide.

DISCUSSION

Using RV-mediated retrograde tracing to label GABAergic neurons innervating wake-promoting neurons and glutamatergic neurons innervating sleep-promoting neurons, we have identified multiple groups of candidate sleep neurons. Bidirectional optogenetic manipulation validated NTS neurons in both the

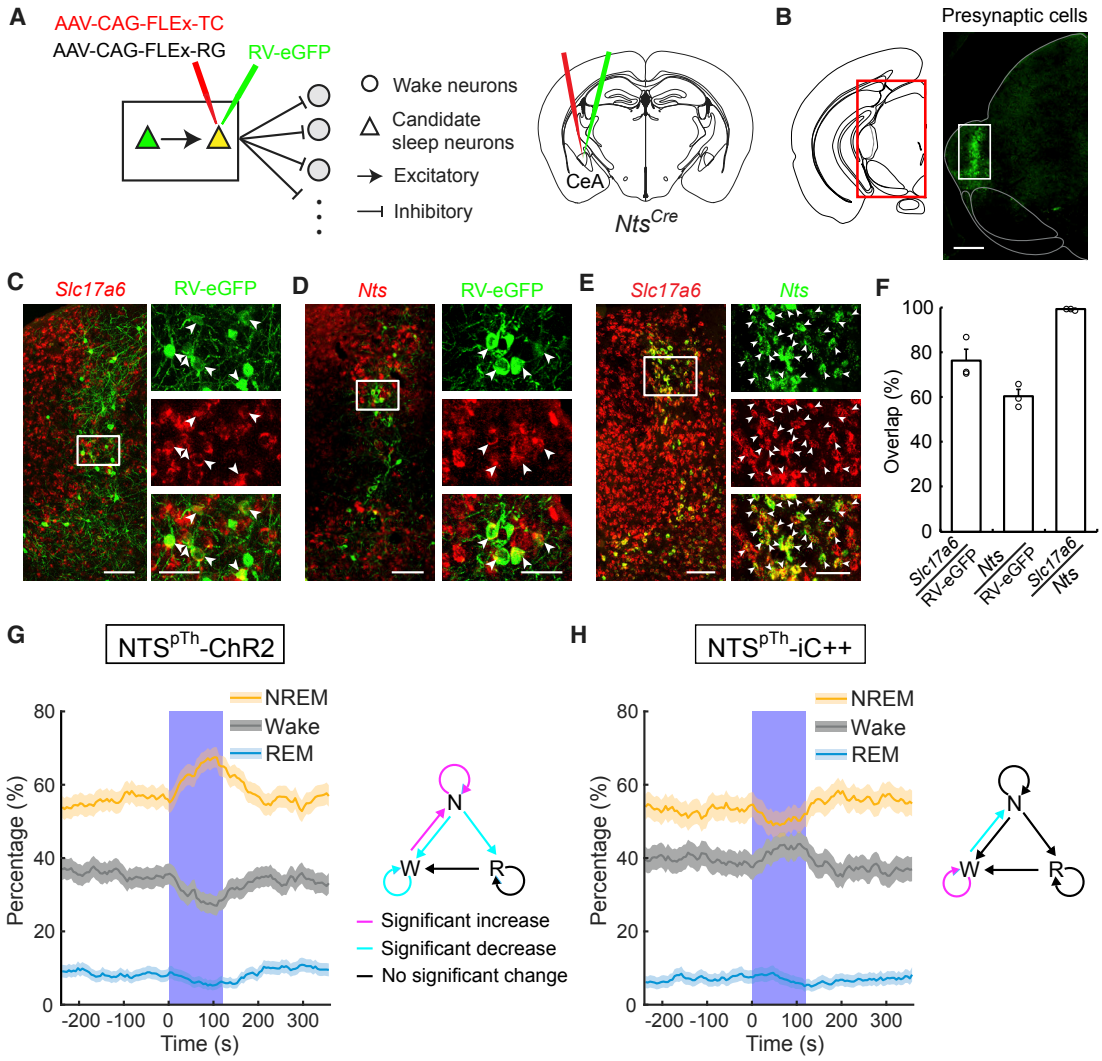

Figure 5. Identification of Glutamatergic Sleep Neurons in the Posterior Thalamus

(A) Schematic for identifying candidate sleep neurons that excite other sleep-promoting neurons using RV-mediated retrograde tracing.

(B) Retrograde tracing from CeA NTS neurons revealed presynaptic neurons in a posterior region of the thalamus. Red box in the coronal diagram indicates the region shown in the fluorescence image; white box in the image indicates the region shown in (C)–(E).

(C–E) RV-labeled posterior thalamic neurons express VGLUT2 and NTS. Shown are fluorescence images of RV-labeled neurons with progressively higher magnification (white box, region enlarged on the right). Arrowheads indicate overlap between RV-EGFP (green) and *Slc17a6* (red, C) or *Nts* (red, D) or between *Nts* (green) and *Slc17a6* (red, E). Scale bars represent 100 μm (low magnification) or 50 μm (high magnification).

(F) Percentage of RV-EGFP cells that express *Slc17a6* or *Nts*, and the percentage of *Nts* cells that express *Slc17a6* (n = 3 mice for each comparison).

(G) Percentage of time in NREM, REM, or the wake state before, during, and after laser stimulation of posterior thalamic NTS neurons (NTS^{pTh}), averaged from 10 mice. Laser stimulation significantly increased NREM sleep ($p < 0.0001$, bootstrap) and decreased wakefulness ($p < 0.0001$) and REM sleep ($p < 0.05$). Shading represents 95% CI. Blue stripe indicates the laser stimulation period (10 Hz, 120 s).

(H) Similar to (G), but for iC++-mediated inactivation. Laser stimulation (constant light, 120 s) significantly decreased NREM sleep ($p < 0.05$, bootstrap) and increased wakefulness ($p < 0.01$, n = 7 mice).

See also Figures S4 and S5.

posterior CeA and the posterior thalamus as NREM-promoting neurons. While the current study focused on CeA GABAergic neurons and their glutamatergic inputs, our initial screening has identified additional candidate sleep neurons (Figure 1B), some of which remain to be functionally tested. The three-step approach used in this study—anatomical screening, marker identification, and functional validation (Figures 1, 2, 3, 4, and 5)—can also be expanded to more wake- or sleep-promoting populations to identify additional neurons in the sleep-control network.

The CeA has been implicated in multiple functions, including the control of fear, anxiety, feeding, and other appetitive behaviors (Cai et al., 2014; Carter et al., 2013; Ciocchi et al., 2010; Douglass et al., 2017; Fadok et al., 2017; Haubensak et al.,

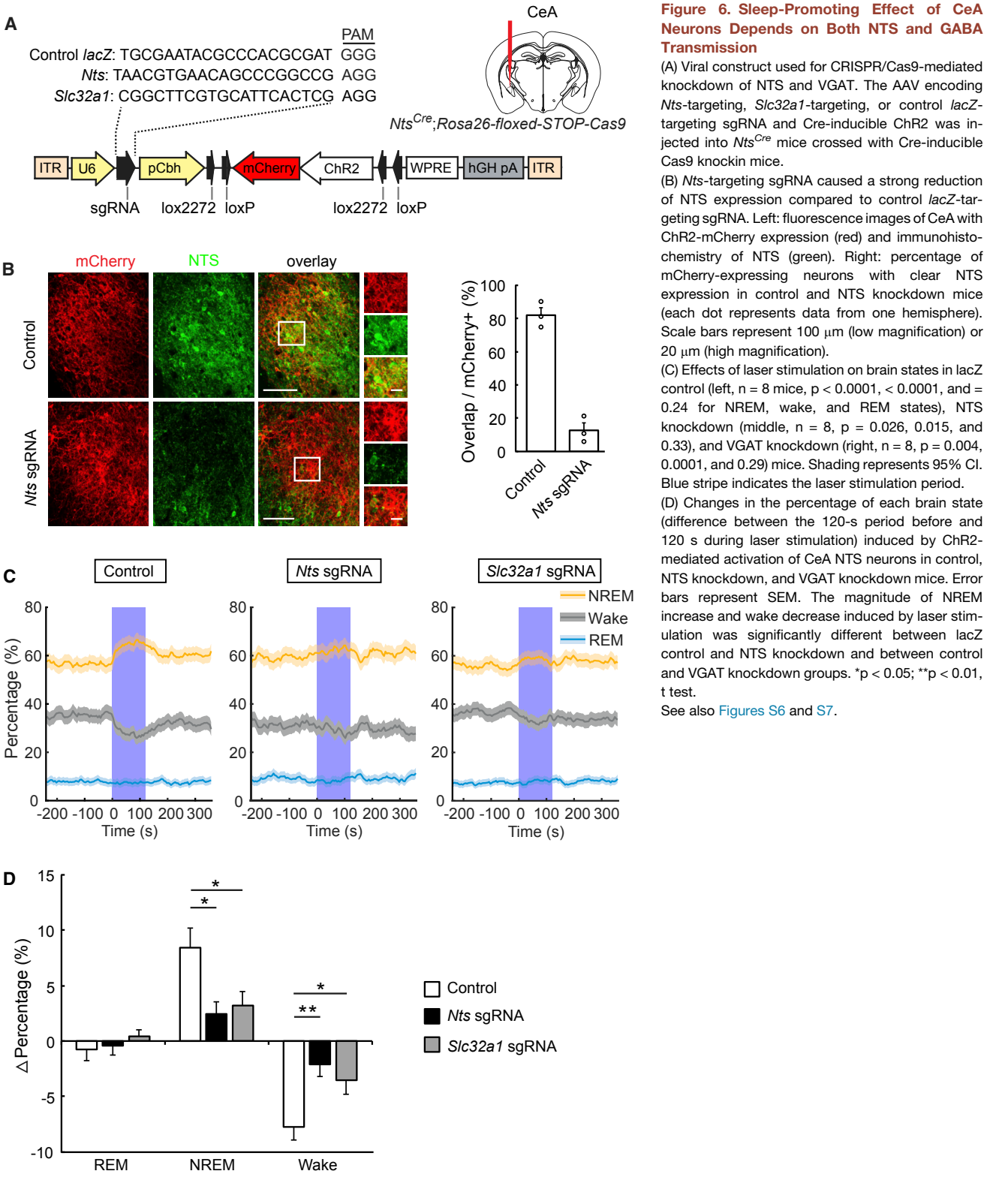

Figure 6. Sleep-Promoting Effect of CeA Neurons Depends on Both NTS and GABA Transmission

(A) Viral construct used for CRISPR/Cas9-mediated knockdown of NTS and VGAT. The AAV encoding *Nts*-targeting, *Slc32a1*-targeting, or control *lacZ*-targeting sgRNA and Cre-inducible ChR2 was injected into Nts^{Cre} mice crossed with Cre-inducible Cas9 knockin mice.

(B) *Nts*-targeting sgRNA caused a strong reduction of NTS expression compared to control *lacZ*-targeting sgRNA. Left: fluorescence images of CeA with ChR2-mCherry expression (red) and immunohistochemistry of NTS (green). Right: percentage of mCherry-expressing neurons with clear NTS expression in control and NTS knockdown mice (each dot represents data from one hemisphere). Scale bars represent 100 μm (low magnification) or 20 μm (high magnification).

(C) Effects of laser stimulation on brain states in lacZ control (left, n = 8 mice, $p < 0.0001$, < 0.0001, and $= 0.24$ for NREM, wake, and REM states), NTS knockdown (middle, n = 8, $p = 0.026$, 0.015, and 0.33), and VGAT knockdown (right, n = 8, $p = 0.004$, 0.0001, and 0.29) mice. Shading represents 95% CI. Blue stripe indicates the laser stimulation period.

(D) Changes in the percentage of each brain state (difference between the 120-s period before and 120 s during laser stimulation) induced by ChR2-mediated activation of CeA NTS neurons in control, NTS knockdown, and VGAT knockdown mice. Error bars represent SEM. The magnitude of NREM increase and wake decrease induced by laser stimulation was significantly different between lacZ control and NTS knockdown and between control and VGAT knockdown groups. *$p < 0.05$; **$p < 0.01$, t test.

See also Figures S6 and S7.

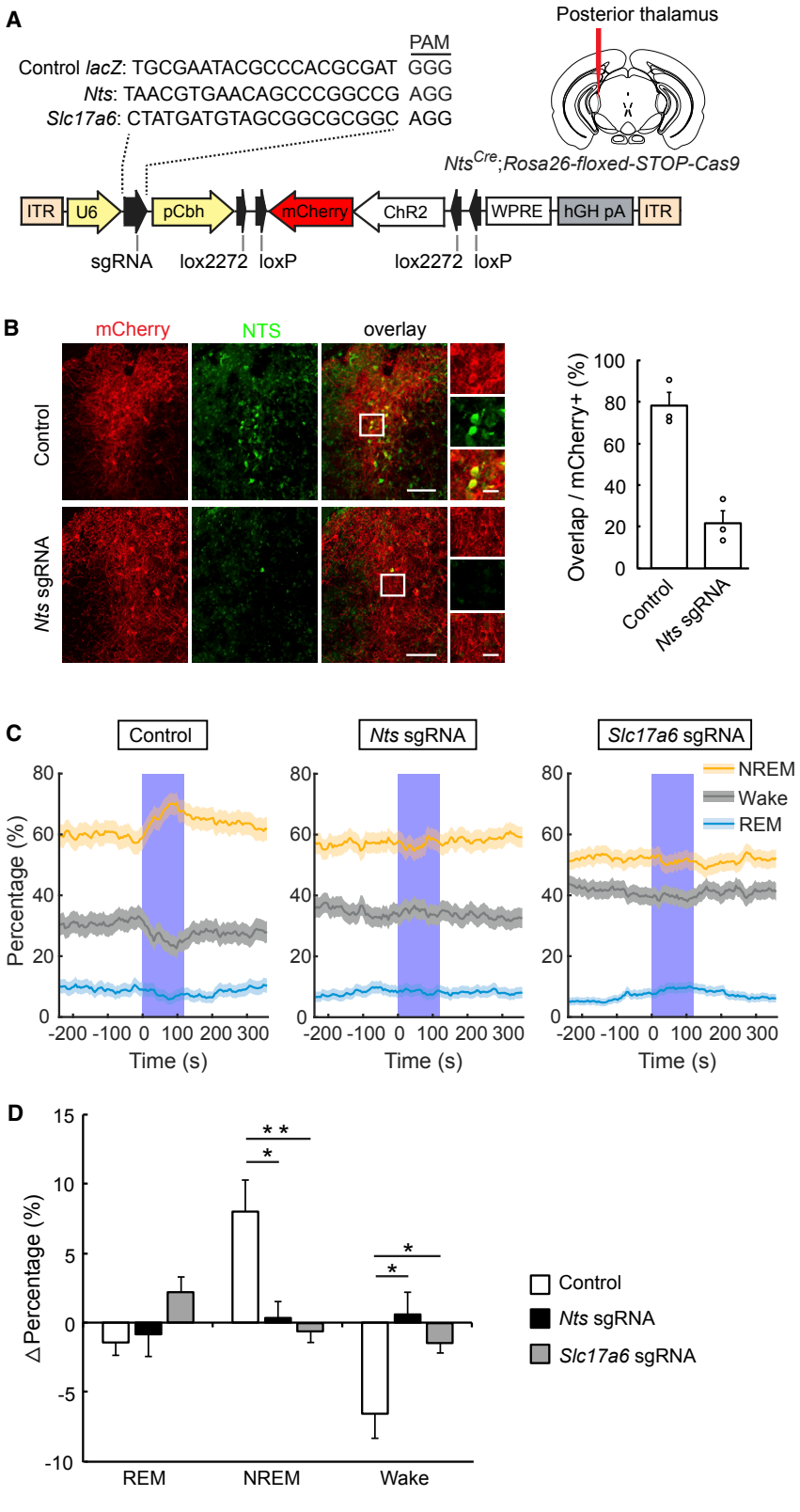

Figure 7. Sleep-Promoting Effect of Posterior Thalamic Neurons Depends on Both NTS and Glutamate Transmission

(A) Viral construct used for CRISPR/Cas9-mediated knockdown of NTS and VGLUT2 in posterior thalamic neurons.

(B) *Nts*-targeting sgRNA caused a strong reduction of NTS expression compared to control *lacZ*-targeting sgRNA. Left: fluorescence images of posterior thalamus with ChR2-mCherry expression (red) and immunohistochemistry of NTS (green). Right: percentage of mCherry-expressing neurons with clear NTS expression in control and NTS knockdown mice (each dot represents data from one hemisphere). Scale bars represent 100 μm (low magnification) or 20 μm (high magnification).

(C) Effects of laser stimulation on brain states in lacZ control (left, n = 5 mice, $p < 0.0001$, < 0.0001, and $= 0.058$ for NREM, wake, and REM states), NTS knockdown (middle, n = 6, $p = 0.42$, 0.21, and 0.27), and VGLUT2 knockdown (right, n = 6, $p = 0.26$, 0.036, and 0.003) mice. Shading represents 95% CI. Blue stripe indicates the laser stimulation period.

(D) Changes in the percentage of each brain state (difference between the 120-s period before and 120 s during laser stimulation) induced by ChR2-mediated activation of posterior thalamic NTS neurons in control, NTS knockdown, and VGLUT2 knockdown mice. Error bars represent SEM. The magnitude of NREM increase and wake decrease induced by laser stimulation was significantly different between lacZ control and NTS knockdown and between control and VGLUT2 knockdown groups. *$p < 0.05$; **$p < 0.01$, t test.

See also Figures S6 and S7.

2010; Janak and Tye, 2015; Kim et al., 2017; Li et al., 2013; McCall et al., 2015; Viviani et al., 2011) as well as REM sleep (Sanford et al., 2002) and cataplexy (Mahoney et al., 2017). Our study demonstrates its causal role in promoting NREM sleep. There are multiple cell types in the CeA, expressing different neuropeptides, and they are likely involved in different functions. A recent study showed the involvement of corticotropin-releasing hormone (*Crh*)$^{+}$*Tac2*$^{+}$*Nts*$^{+}$ CeL neurons in appetitive behaviors in food- or water-deprived mice (Kim et al., 2017). In our experiments in mice with free access to food and water, NTS neuron activation and inactivation promoted and suppressed NREM sleep, respectively (Figure 3). These different effects may be related to the different behavioral contexts or different CeL subregions targeted in the two studies. In future studies, it would be interesting to explore whether and how CeA neurons mediate the interaction between appetitive behaviors (e.g., feeding and drinking), emotional processing, and sleep (Krause et al., 2017; Yamashita and Yamanaka, 2017). Furthermore, a significant fraction of the CeA neurons innervating wake-promoting populations are non-NTS cells (Figure 2D), which may also contribute to sleep regulation. These may include PDYN- or TAC2-positive but NTS-negative neurons or neurons expressing the non-peptide markers identified in the gene-profiling experiment (Figure 2B). Both the genetic identity and functional importance of these neurons await future investigation.

The sleep-promoting effect of CeA NTS neurons is likely mediated in part by their broad GABAergic inhibition of multiple wake-promoting populations (Brown et al., 2012; Saper et al., 2010; Scammell et al., 2017; Weber and Dan, 2016) (Figure S2). Upstream to these CeA neurons, a major population of glutamatergic sleep neurons was found in the posterior thalamus (Figure 5). While their excitatory innervation of the CeA neurons is likely to contribute to the sleep-promoting effect, these thalamic neurons also send axon projections to other brain regions, some of which may also participate in sleep regulation.

Apart from the traditional neurotransmitters, glutamate and GABA, the posterior thalamic and CeA neurons both contain neuropeptides, and NTS knockdown in each population greatly reduced their sleep-promoting effect (Figures 6 and 7). This is consistent with the negative impact of NTS receptor 1 knockout on sleep (Fitzpatrick et al., 2012), indicating that NTS signaling plays an important role in sleep generation. Interestingly, the NTS peptide is also known to lower the blood pressure and body temperature (Bissette et al., 1982; Carraway and Leeman, 1973), processes naturally associated with NREM sleep (Alföldi et al., 1990; Jafari, 2017; Silvani and Dampney, 2013). This suggests that the NTS-releasing neurons could serve to coordinate NREM sleep generation and the associated autonomic regulation.

Like many other neuropeptides, NTS may act through local synaptic transmission and/or diffuse volume transmission (van den Pol, 2012). In future studies, it would be important to determine whether the peptides released by the CeA and pTh act on the same neurons that receive the GABAergic and glutamatergic innervation, respectively. Through volume transmission, it is even possible that NTS released by different brain regions acts on common neuronal targets. In addition to the CeA and posterior thalamus, NTS-expressing neurons are distributed in multiple other brain regions (2011 Allen Institute for Cell Science, Allen Mouse Brain Atlas, available at http://mouse.brain-map.org/experiment/show/73788032), many of which are closely associated with the central autonomic network. Our finding that the two populations along the thalamo-amygdala pathway both promote NREM sleep raises the possibility that NTS may serve as a common marker for multiple neuronal groups in the sleep-control network.

STAR★METHODS

Detailed methods are provided in the online version of this paper and include the following:

- KEY RESOURCES TABLE
- CONTACT FOR REAGENT AND RESOURCE SHARING
- EXPERIMENTAL MODEL AND SUBJECT DETAILS
  - Animals
- METHOD DETAILS
  - Virus preparation
  - Surgery
  - Polysomnographic recordings
  - Sleep deprivation and rebound
  - Optogenetic manipulation
  - Optrode recording
  - Immunohistochemistry and immunocytochemistry
  - Fluorescence *in situ* hybridization (FISH)
  - Translating ribosome affinity purification (TRAP)
  - CRISPR/Cas9-mediated gene knockdown
  - Slice recording
  - Single-cell RT-PCR
- QUANTIFICATION AND STATISTICAL ANALYSIS
- DATA AND SOFTWARE AVAILABILITY

SUPPLEMENTAL INFORMATION

Supplemental Information can be found online at https://doi.org/10.1016/j.neuron.2019.05.015.

ACKNOWLEDGMENTS

We thank Martin Myers for generously providing the *Nts*^{Cre} mice, Lin He for generously providing the Cas9-expressing 368T1 cell line, Alexander R. Nectow for technical advice on TRAP RNA-seq experiments, Hui Yang for technical advice on CRISPR experiments, Justin Y. Choi and Karen Lundy (Functional Genomics Laboratory, University of California, Berkeley) for help with RNA-seq library preparation and sequencing, Bo Li and Michael Cole for help with RNA-seq data analysis, and the Viral Cores at the University of North Carolina, Stanford University, Salk Institute, McGovern Institute for Brain Research at MIT, and Addgene for supplying AAV, HSV, and RV. This work was supported by the Howard Hughes Medical Institute.

AUTHOR CONTRIBUTIONS

C.M. and Y.D. conceived and designed the study and wrote the paper. C.M. performed most of the experiments. P.Z. and L.Z. performed and analyzed the data for slice recordings. D.L. and Z.K.B. wrote programs for data analysis, and C.M. and Z.K.B. analyzed the data. W.-C.C. and C.M. produced virus for RV tracing. B.K. performed some brain tissue sectioning. Y.D. supervised all aspects of the work.

DECLARATION OF INTERESTS

The authors declare no competing interests.

Received: December 5, 2018
Revised: April 15, 2019
Accepted: May 7, 2019
Published: June 6, 2019

REFERENCES

Alföldi, P., Rubicsek, G., Cserni, G., and Obál, F., Jr. (1990). Brain and core temperatures and peripheral vasomotion during sleep and wakefulness at various ambient temperatures in the rat. Pflugers Arch. *417*, 336–341.

Anaclet, C., Ferrari, L., Arrigoni, E., Bass, C.E., Saper, C.B., Lu, J., and Fuller, P.M. (2014). The GABAergic parafacial zone is a medullary slow wave sleep-promoting center. Nat. Neurosci. *17*, 1217–1224.

Anikeeva, P., Andalman, A.S., Witten, I., Warden, M., Goshen, I., Grosenick, L., Gunaydin, L.A., Frank, L.M., and Deisseroth, K. (2011). Optetrode: a multichannel readout for optogenetic control in freely moving mice. Nat. Neurosci. *15*, 163–170.

Beier, K.T., Steinberg, E.E., DeLoach, K.E., Xie, S., Miyamichi, K., Schwarz, L., Gao, X.J., Kremer, E.J., Malenka, R.C., and Luo, L. (2015). Circuit architecture of VTA dopamine neurons revealed by systematic input-output mapping. Cell *162*, 622–634.

Bissette, G., Luttinger, D., Mason, G.A., Hernandez, D.E., and Loosen, P.T. (1982). Neurotensin and thermoregulation. Ann. NY Acad. Sci. *400*, 268–282.

Brown, R.E., Basheer, R., McKenna, J.T., Strecker, R.E., and McCarley, R.W. (2012). Control of sleep and wakefulness. Physiol. Rev. *92*, 1087–1187.

Cai, H., Haubensak, W., Anthony, T.E., and Anderson, D.J. (2014). Central amygdala PKC-δ(+) neurons mediate the influence of multiple anorexigenic signals. Nat. Neurosci. *17*, 1240–1248.

Carraway, R., and Leeman, S.E. (1973). The isolation of a new hypotensive peptide, neurotensin, from bovine hypothalami. J. Biol. Chem. *248*, 6854–6861.

Carter, M.E., Soden, M.E., Zweifel, L.S., and Palmiter, R.D. (2013). Genetic identification of a neural circuit that suppresses appetite. Nature *503*, 111–114.

Chung, S., Weber, F., Zhong, P., Tan, C.L., Nguyen, T.N., Beier, K.T., Hörmann, N., Chang, W.C., Zhang, Z., Do, J.P., et al. (2017). Identification of preoptic sleep neurons using retrograde labelling and gene profiling. Nature *545*, 477–481.

Ciocchi, S., Herry, C., Grenier, F., Wolff, S.B., Letzkus, J.J., Vlachos, I., Ehrlich, I., Sprengel, R., Deisseroth, K., Stadler, M.B., et al. (2010). Encoding of conditioned fear in central amygdala inhibitory circuits. Nature *468*, 277–282.

Douglass, A.M., Kucukdereli, H., Ponserre, M., Markovic, M., Gründemann, J., Strobel, C., Alcala Morales, P.L., Conzelmann, K.K., Lüthi, A., and Klein, R. (2017). Central amygdala circuits modulate food consumption through a positive-valence mechanism. Nat. Neurosci. *20*, 1384–1394.

Eban-Rothschild, A., Rothschild, G., Giardino, W.J., Jones, J.R., and de Lecea, L. (2016). VTA dopaminergic neurons regulate ethologically relevant sleep-wake behaviors. Nat. Neurosci. *19*, 1356–1366.

Ekstrand, M.I., Nectow, A.R., Knight, Z.A., Latcha, K.N., Pomeranz, L.E., and Friedman, J.M. (2014). Molecular profiling of neurons based on connectivity. Cell *157*, 1230–1242.

Fadok, J.P., Krabbe, S., Markovic, M., Courtin, J., Xu, C., Massi, L., Botta, P., Bylund, K., Müller, C., Kovacevic, A., et al. (2017). A competitive inhibitory circuit for selection of active and passive fear responses. Nature *542*, 96–100.

Fitzpatrick, K., Winrow, C.J., Gotter, A.L., Millstein, J., Arbuzova, J., Brunner, J., Kasarskis, A., Vitaterna, M.H., Renger, J.J., and Turek, F.W. (2012). Altered sleep and affect in the neurotensin receptor 1 knockout mouse. Sleep (Basel) *35*, 949–956.

Haubensak, W., Kunwar, P.S., Cai, H., Ciocchi, S., Wall, N.R., Ponnusamy, R., Biag, J., Dong, H.W., Deisseroth, K., Callaway, E.M., et al. (2010). Genetic dissection of an amygdala microcircuit that gates conditioned fear. Nature *468*, 270–276.

Hauswirth, W.W., Lewin, A.S., Zolotukhin, S., and Muzyczka, N. (2000). Production and purification of recombinant adeno-associated virus. Methods Enzymol. *316*, 743–761.

Heiman, M., Schaefer, A., Gong, S., Peterson, J.D., Day, M., Ramsey, K.E., Suárez-Fariñas, M., Schwarz, C., Stephan, D.A., Surmeier, D.J., et al. (2008). A translational profiling approach for the molecular characterization of CNS cell types. Cell *135*, 738–748.

Heiman, M., Kulicke, R., Fenster, R.J., Greengard, P., and Heintz, N. (2014). Cell type-specific mRNA purification by translating ribosome affinity purification (TRAP). Nat. Protoc. *9*, 1282–1291.

Jafari, B. (2017). Sleep architecture and blood pressure. Sleep Med. Clin. *12*, 161–166.

Janak, P.H., and Tye, K.M. (2015). From circuits to behaviour in the amygdala. Nature *517*, 284–292.

Jego, S., Glasgow, S.D., Herrera, C.G., Ekstrand, M., Reed, S.J., Boyce, R., Friedman, J., Burdakov, D., and Adamantidis, A.R. (2013). Optogenetic identification of a rapid eye movement sleep modulatory circuit in the hypothalamus. Nat. Neurosci. *16*, 1637–1643.

Kim, T., and Kerschensteiner, D. (2017). Inhibitory control of feature selectivity in an object motion sensitive circuit of the retina. Cell Rep. *19*, 1343–1350.

Kim, J., Zhang, X., Muralidhar, S., LeBlanc, S.A., and Tonegawa, S. (2017). Basolateral to central amygdala neural circuits for appetitive behaviors. Neuron *93*, 1464–1479.e1465.

Konadhode, R.R., Pelluru, D., Blanco-Centurion, C., Zayachkivsky, A., Liu, M., Uhde, T., Glen, W.B., Jr., van den Pol, A.N., Mulholland, P.J., and Shiromani, P.J. (2013). Optogenetic stimulation of MCH neurons increases sleep. J. Neurosci. *33*, 10257–10263.

Krause, A.J., Simon, E.B., Mander, B.A., Greer, S.M., Saletin, J.M., Goldstein-Piekarski, A.N., and Walker, M.P. (2017). The sleep-deprived human brain. Nat. Rev. Neurosci. *18*, 404–418.

Leinninger, G.M., Opland, D.M., Jo, Y.H., Faouzi, M., Christensen, L., Cappellucci, L.A., Rhodes, C.J., Gnegy, M.E., Becker, J.B., Pothos, E.N., et al. (2011). Leptin action via neurotensin neurons controls orexin, the mesolimbic dopamine system and energy balance. Cell Metab. *14*, 313–323.

Li, B., and Dewey, C.N. (2011). RSEM: accurate transcript quantification from RNA-seq data with or without a reference genome. BMC Bioinformatics *12*, 323.

Li, H., Penzo, M.A., Taniguchi, H., Kopec, C.D., Huang, Z.J., and Li, B. (2013). Experience-dependent modification of a central amygdala fear circuit. Nat. Neurosci. *16*, 332–339.

Liu, K., Kim, J., Kim, D.W., Zhang, Y.S., Bao, H., Denaxa, M., Lim, S.A., Kim, E., Liu, C., Wickersham, I.R., et al. (2017). Lhx6-positive GABA-releasing neurons of the zona incerta promote sleep. Nature *548*, 582–587.

Lu, J., Greco, M.A., Shiromani, P., and Saper, C.B. (2000). Effect of lesions of the ventrolateral preoptic nucleus on NREM and REM sleep. J. Neurosci. *20*, 3830–3842.

Mahoney, C.E., Agostinelli, L.J., Brooks, J.N., Lowell, B.B., and Scammell, T.E. (2017). GABAergic neurons of the central amygdala promote cataplexy. J. Neurosci. *37*, 3995–4006.

McCall, J.G., Al-Hasani, R., Siuda, E.R., Hong, D.Y., Norris, A.J., Ford, C.P., and Bruchas, M.R. (2015). CRH engagement of the locus coeruleus noradrenergic system mediates stress-induced anxiety. Neuron *87*, 605–620.

Nauta, W.J. (1946). Hypothalamic regulation of sleep in rats; an experimental study. J. Neurophysiol. *9*, 285–316.

Nectow, A.R., Ekstrand, M.I., and Friedman, J.M. (2015). Molecular characterization of neuronal cell types based on patterns of projection with Retro-TRAP. Nat. Protoc. *10*, 1319–1327.

Oishi, Y., Xu, Q., Wang, L., Zhang, B.J., Takahashi, K., Takata, Y., Luo, Y.J., Cherasse, Y., Schiffmann, S.N., de Kerchove d'Exaerde, A., et al. (2017).

Slow-wave sleep is controlled by a subset of nucleus accumbens core neurons in mice. Nat. Commun. *8*, 734.

Osakada, F., and Callaway, E.M. (2013). Design and generation of recombinant rabies virus vectors. Nat. Protoc. *8*, 1583–1601.

Paul, A., Crow, M., Raudales, R., He, M., Gillis, J., and Huang, Z.J. (2017). Transcriptional architecture of synaptic communication delineates GABAergic neuron identity. Cell *171*, 522–539.e520.

Penzo, M.A., Robert, V., Tucciarone, J., De Bundel, D., Wang, M., Van Aelst, L., Darvas, M., Parada, L.F., Palmiter, R.D., He, M., et al. (2015). The paraventricular thalamus controls a central amygdala fear circuit. Nature *519*, 455–459.

Platt, R.J., Chen, S., Zhou, Y., Yim, M.J., Swiech, L., Kempton, H.R., Dahlman, J.E., Parnas, O., Eisenhaure, T.M., Jovanovic, M., et al. (2014). CRISPR-Cas9 knockin mice for genome editing and cancer modeling. Cell *159*, 440–455.

Rau, A.R., and Hentges, S.T. (2017). The relevance of AgRP neuron-derived GABA inputs to POMC neurons differs for spontaneous and evoked release. J. Neurosci. *37*, 7362–7372.

Ren, S., Wang, Y., Yue, F., Cheng, X., Dang, R., Qiao, Q., Sun, X., Li, X., Jiang, Q., Yao, J., et al. (2018). The paraventricular thalamus is a critical thalamic area for wakefulness. Science *362*, 429–434.

Sallanon, M., Denoyer, M., Kitahama, K., Aubert, C., Gay, N., and Jouvet, M. (1989). Long-lasting insomnia induced by preoptic neuron lesions and its transient reversal by muscimol injection into the posterior hypothalamus in the cat. Neuroscience *32*, 669–683.

Sanford, L.D., Parris, B., and Tang, X. (2002). GABAergic regulation of the central nucleus of the amygdala: implications for sleep control. Brain Res. *956*, 276–284.

Saper, C.B., Fuller, P.M., Pedersen, N.P., Lu, J., and Scammell, T.E. (2010). Sleep state switching. Neuron *68*, 1023–1042.

Scammell, T.E., Arrigoni, E., and Lipton, J.O. (2017). Neural circuitry of wakefulness and sleep. Neuron *93*, 747–765.

Schweizer, N., Pupe, S., Arvidsson, E., Nordenankar, K., Smith-Anttila, C.J., Mahmoudi, S., Andrén, A., Dumas, S., Rajagopalan, A., Lévesque, D., et al. (2014). Limiting glutamate transmission in a Vglut2-expressing subpopulation of the subthalamic nucleus is sufficient to cause hyperlocomotion. Proc. Natl. Acad. Sci. USA *111*, 7837–7842.

Shen, H., Marino, R.A.M., McDevitt, R.A., Bi, G.H., Chen, K., Madeo, G., Lee, P.T., Liang, Y., De Biase, L.M., Su, T.P., et al. (2018). Genetic deletion of vesicular glutamate transporter in dopamine neurons increases vulnerability to MPTP-induced neurotoxicity in mice. Proc. Natl. Acad. Sci. USA *115*, E11532–E11541.

Sherin, J.E., Elmquist, J.K., Torrealba, F., and Saper, C.B. (1998). Innervation of histaminergic tuberomammillary neurons by GABAergic and galaninergic neurons in the ventrolateral preoptic nucleus of the rat. J. Neurosci. *18*, 4705–4721.

Silvani, A., and Dampney, R.A. (2013). Central control of cardiovascular function during sleep. Am. J. Physiol. Heart Circ. Physiol. *305*, H1683–H1692.

Steininger, T.L., Gong, H., McGinty, D., and Szymusiak, R. (2001). Subregional organization of preoptic area/anterior hypothalamic projections to arousal-related monoaminergic cell groups. J. Comp. Neurol. *429*, 638–653.

Tsunematsu, T., Ueno, T., Tabuchi, S., Inutsuka, A., Tanaka, K.F., Hasuwa, H., Kilduff, T.S., Terao, A., and Yamanaka, A. (2014). Optogenetic manipulation of activity and temporally controlled cell-specific ablation reveal a role for MCH neurons in sleep/wake regulation. J. Neurosci. *34*, 6896–6909.

van den Pol, A.N. (2012). Neuropeptide transmission in brain circuits. Neuron *76*, 98–115.

Viviani, D., Charlet, A., van den Burg, E., Robinet, C., Hurni, N., Abatis, M., Magara, F., and Stoop, R. (2011). Oxytocin selectively gates fear responses through distinct outputs from the central amygdala. Science *333*, 104–107.

Von Economo, C. (1930). Sleep as a problem of localization. J. Nerv. Ment. Dis. *71*, 249–259.

Weber, F., and Dan, Y. (2016). Circuit-based interrogation of sleep control. Nature *538*, 51–59.

Weber, F., Chung, S., Beier, K.T., Xu, M., Luo, L., and Dan, Y. (2015). Control of REM sleep by ventral medulla GABAergic neurons. Nature *526*, 435–438.

Weissbourd, B., Ren, J., DeLoach, K.E., Guenthner, C.J., Miyamichi, K., and Luo, L. (2014). Presynaptic partners of dorsal raphe serotonergic and GABAergic neurons. Neuron *83*, 645–662.

Wickersham, I.R., Lyon, D.C., Barnard, R.J., Mori, T., Finke, S., Conzelmann, K.K., Young, J.A., and Callaway, E.M. (2007). Monosynaptic restriction of transsynaptic tracing from single, genetically targeted neurons. Neuron *53*, 639–647.

Xu, M., Chung, S., Zhang, S., Zhong, P., Ma, C., Chang, W.C., Weissbourd, B., Sakai, N., Luo, L., Nishino, S., and Dan, Y. (2015). Basal forebrain circuit for sleep-wake control. Nat. Neurosci. *18*, 1641–1647.

Yamashita, T., and Yamanaka, A. (2017). Lateral hypothalamic circuits for sleep-wake control. Curr. Opin. Neurobiol. *44*, 94–100.

Yang, S.R., Hu, Z.Z., Luo, Y.J., Zhao, Y.N., Sun, H.X., Yin, D., Wang, C.Y., Yan, Y.D., Wang, D.R., Yuan, X.S., et al. (2018). The rostromedial tegmental nucleus is essential for non-rapid eye movement sleep. PLoS. Biol. *16*, e2002909.

Yu, X., Li, W., Ma, Y., Tossell, K., Harris, J.J., Harding, E.C., Ba, W., Miracca, G., Wang, D., Li, L., et al. (2019). GABA and glutamate neurons in the VTA regulate sleep and wakefulness. Nat. Neurosci. *22*, 106–119.

Yuan, X.S., Wang, L., Dong, H., Qu, W.M., Yang, S.R., Cherasse, Y., Lazarus, M., Schiffmann, S.N., d'Exaerde, A.K., Li, R.X., and Huang, Z.L. (2017). Striatal adenosine A_{2A} receptor neurons control active-period sleep via parvalbumin neurons in external globus pallidus. eLife *6*, e29055.

Zelikowsky, M., Hui, M., Karigo, T., Choe, A., Yang, B., Blanco, M.R., Beadle, K., Gradinaru, V., Deverman, B.E., and Anderson, D.J. (2018). The neuropeptide Tac2 controls a distributed brain state induced by chronic social isolation stress. Cell *173*, 1265–1279.e1219.

Zhang, Z., Ferretti, V., Güntan, İ., Moro, A., Steinberg, E.A., Ye, Z., Zecharia, A.Y., Yu, X., Vyssotski, A.L., Brickley, S.G., et al. (2015). Neuronal ensembles sufficient for recovery sleep and the sedative actions of $\alpha 2$ adrenergic agonists. Nat. Neurosci. *18*, 553–561.

Zhu, Y., Nachtrab, G., Keyes, P.C., Allen, W.E., Luo, L., and Chen, X. (2018). Dynamic salience processing in paraventricular thalamus gates associative learning. Science *362*, 423–429.

STAR★METHODS

KEY RESOURCES TABLE

REAGENT or RESOURCE	SOURCE	IDENTIFIER
Antibodies		
Chicken anti-GFP	Aves Labs	Cat# GFP-1020; RRID: AB_10000240
Sheep alkaline phosphatase-conjugated anti-DIG antibody	Roche Applied Science	Cat# 11093274910; RRID: AB_514497
Rat anti-mCherry	Thermo Fisher Scientific	Cat# M11217; RRID: AB_2536611
Rabbit anti-c-Fos	Synaptic System	Cat# 226003; RRID: AB_2231974
Rabbit anti-NTS	ImmunoStar	Cat# 20072; RRID: AB_572254
Mouse anti-FLAG	Sigma-Aldrich	Cat# F1804; RRID: AB_262044
Rabbit anti-HA	Cell Signaling Technology	Cat# 3724; RRID: AB_1549585
Rabbit anti-TH	Abcam	Cat# AB112; RRID: AB_297840
Bacterial and Virus Strains		
AAV2-EF1α-DIO-ChR2-eYFP	UNC Chapel Hill Vector Core	N/A
AAVDJ-EF1α-DIO-ChR2-eYFP	Stanford University Virus Core	N/A
AAV2-EF1α-DIO-iC++-eYFP	UNC Chapel Hill Vector Core	N/A
AAV2-EF1α-DIO-eYFP	UNC Chapel Hill Vector Core	N/A
AAV2-CAG-FLEx-TC	Gift from Liqun Luo lab, Stanford University	N/A
AAV2-CAG-FLEx-RG	Gift from Liquan Luo lab, Stanford University	N/A
G-Deleted rabies-eGFP	Gene Transfer Targeting and Therapeutics Core of Salk Institute	N/A
HSV-hEF1α-LoxSTOPLox (LSL)-FlagHA-L10a	MIT viral core	N/A
AAV2-U6-DIO-lacZ sgRNA-pCbh-Dio-ChR2-mCherry	This paper	N/A
AAV2-U6-DIO-*Nts* sgRNA-pCbh-Dio-ChR2-mCherry	This paper	N/A
AAV2-U6-DIO-*Slc32a1* sgRNA-pCbh-Dio-ChR2-mCherry	This paper	N/A
AAV2-U6-DIO-*Slc17a6* sgRNA-pCbh-Dio-ChR2-mCherry	This paper	N/A
Chemicals, Peptides, and Recombinant Proteins		
Fast Red TR/Naphthol AS-MX Tablets	Sigma-Aldrich	Cat# F4523
Protein A Dynabeads	Thermo Fisher Scientific	Cat# 10002D
Bicuculline	Sigma-Aldrich	Cat# 14340
Critical Commercial Assays		
Absolutely RNA Nanoprep kit	Agilent	Cat# 400753
SuperScript III kit	Invitrogen	Cat# 18080-051
Accuprime Taq polymerase	Invitrogen	Cat# 12339-024
GoTaq Green Master Mix	Promega	Cat# M7122
RNAscope Manual Fluorescent Multiplex kit V2	Advanced Cell Diagnostics	Cat# 323100
Alexa Fluor 488 Tyramide SuperBoost Kit	Thermo Fisher Scientific	Cat# B40922
Deposited Data		
Raw and analyzed TRAP RNA-seq data	This paper	GEO: GSE121888
Experimental Models: Cell Lines		
Hamster: B7GG cells	Gene Transfer Targeting and Therapeutics Core of Salk Institute	N/A
Hamster: BHK-EnvA cells	Gene Transfer Targeting and Therapeutics Core of Salk Institute	N/A
Human: HEK293-TVA cells	Gene Transfer Targeting and Therapeutics Core of Salk Institute	N/A

(*Continued on next page*)

Continued

REAGENT or RESOURCE	SOURCE	IDENTIFIER
Human: HEK293T cells	Gift from Liqun Luo lab, Stanford University	N/A
Mouse: 368T1 Cas9-expressing cells	Gift from Lin He lab, UC Berkeley	N/A
Experimental Models: Organisms/Strains		
Mouse, *Slc17a6*^{Cre}	The Jackson Laboratory	Cat# 016963; RRID: IMSR_JAX:016963
Mouse, *Chat*^{Cre}	The Jackson Laboratory	Cat# 006410; RRID: IMSR_JAX:006410
Mouse, *Hdc*^{Cre}	The Jackson Laboratory	Cat# 021198; RRID: IMSR_JAX:021198
Mouse, *Pvalb*^{Cre}	The Jackson Laboratory	Cat# 008069; RRID: IMSR_JAX:008069
Mouse, *Nts*^{Cre}	The Jackson Laboratory	Cat# 017525; RRID: IMSR_JAX:017525
Mouse, *Rosa26-floxed-STOP-Cas9*	The Jackson Laboratory	Cat# 024857; RRID: IMSR_JAX:024857
Mouse, *Th*^{Cre}	European Mouse Mutant Archive	Cat# EM:00254; RRID: IMSR_EM:00254
Oligonucleotides		
Primers for cloning FISH probes, please see Table S1	Allen Brain Atlas	N/A
Primers for single-cell RT–PCR, please see Table S2	This paper	N/A
Single guide RNA sequence for *lacZ*: TGCGAATAC GCCCACGCGAT	Addgene	Cat# 60228
Single guide RNA sequence for *Nts;* TAACGTGAA CAGCCCGGCCG	This paper	N/A
Single guide RNA sequence for *Slc32a1:* CGGCTTC GTGCATTCACTCG	This paper	N/A
Single guide RNA sequence for *Slc17a6:* CTATGAT GTAGCGGCGCGGC	This paper	N/A
Recombinant DNA		
pCMV6-Nts-FLAG	OriGene Technologies	Cat# MR226576
pCMV6-Slc32a1-FLAG	OriGene Technologies	Cat# MR208431
pCMV6-Slc17a6-FLAG	OriGene Technologies	Cat# MR209115
pU6-sgRNA(backbone)-pCBh-Cre-WPRE-hGHpA	Addgene	Cat# 60229; RRID: Addgene_60229
Software and Algorithms		
RSEM (RNA-Seq by Expectation-Maximization)	Li and Dewey, 2011	https://github.com/deweylab/RSEM
ImageJ	NIH	https://imagej.nih.gov/ij/
MATLAB	MathWorks	R2014b
KlustaKwik	Kenneth D. Harris	http://klustakwik.sourceforge.net
Other		
eGFP probe for RNAscope assays	Advanced Cell Diagnostics	Cat# 400281
Nts probe for RNAscope assays	Advanced Cell Diagnostics	Cat# 420441
Tac2 probe for RNAscope assays	Advanced Cell Diagnostics	Cat# 446391
Pdyn probe for RNAscope assays	Advanced Cell Diagnostics	Cat# 318771
Gad1 probe for RNAscope assays	Advanced Cell Diagnostics	Cat# 400951
Slc17a6 probe for RNAscope assays	Advanced Cell Diagnostics	Cat# 319171
Cre probe for RNAscope assays	Advanced Cell Diagnostics	Cat# 312281
Fos probe for RNAscope assays	Advanced Cell Diagnostics	Cat# 506921 and 506931
Gbx2 probe for RNAscope assays	Advanced Cell Diagnostics	Cat# 314351
Tcf7l2 probe for RNAscope assays	Advanced Cell Diagnostics	Cat# 466901

CONTACT FOR REAGENT AND RESOURCE SHARING

Further information and requests for resources and reagents should be directed to and will be fulfilled by the Lead Contact, Yang Dan (ydan@berkeley.edu).

EXPERIMENTAL MODEL AND SUBJECT DETAILS

Animals

The following mice were obtained from Jackson Laboratory (Jackson stock number in parenthesis): *Slc17a6*^{Cre} (016963), *Chat*^{Cre} (006410), *Hdc*^{Cre} (021198), *Pvalb*^{Cre} (008069), *Nts*^{Cre} (017525), and *Rosa26-floxed-STOP-Cas9* (024857). *Th*^{Cre} mice were obtained from the European Mouse Mutant Archive (EM:00254). Rabies tracing, gene profiling, optogenetic manipulation, and optrode recording experiments were performed on adult mice (> 2 months) of both genders. Slice recordings were performed on mice older than 1 month of both genders. Mice were housed in 12 h light-dark cycle (lights on 07:00 and off at 19:00) with free access to food and water. All procedures were approved by Animal Care and Use Committees of the University of California, Berkeley and were done in accordance with federal regulations and guidelines on animal experimentation.

METHOD DETAILS

Virus preparation

AAV2-EF1α-DIO-hChR2-eYFP, AAV2-EF1α-DIO-iC++-eYFP, AAV2-EF1α-DIO-eYFP were obtained from the University of North Carolina (UNC) vector core. For RV-mediated circuit tracing, pCAG-FLEx-TC and pCAG-FLEx-RG constructs were generous gifts from Liqun Luo, and AAV2 viruses were packaged in-house according to previously described protocols (Hauswirth et al., 2000). HSV-hEF1α-LoxSTOPLox (LSL)-FlagHA-L10a was obtained from MIT viral core. G-Deleted rabies-eGFP were purchased from Gene Transfer Targeting and Therapeutics Core of Salk Institute, amplified in B7GG cells, pseudotyped with BHK-EnvA cells, and titered with HEK293-TVA cells (Osakada and Callaway, 2013).

Surgery

Adult mice (6-12 weeks old) were anesthetized with 1.5%–2% isoflurane and placed on a stereotaxic frame. Heat pad was used to keep the body temperature stable during the whole procedure. Eye ointment was applied to keep the eyes from drying. After shaving hairs and asepsis with Betadine and medical alcohol, an incision was made to the skin to expose the skull.

For virus injection, a craniotomy was made on top of the target region, and 0.1-0.3 μl virus was injected into the target region using Nanoject II (Drummond Scientific) via a micro pipette. For optogenetic activation/inhibition experiments, AAV2-EF1α-DIO-hChR2-eYFP, AAV2-EF1α-DIO-iC++-eYFP, AAV2-EF1α-DIO-eYFP, or AAV2-U6-sgRNA (*lacZ*, *Nts*, *Slc32a1*, or *Slc17a6*)-pCbh-DIO-ChR2-mCherry was injected into the posterior CeA, posterior thalamus or PVT of *Nts*^{Cre} or *Nts*^{Cre}*;Rosa26-floxed-STOP-Cas9* mice. For rabies tracing, a mixture of AAV2-CAG-FLEx-TVA-mCherry and AAV2-CAG-FLEx-RG was injected into the target region of the corresponding Cre mice. Two to three weeks later, EnvA-pseudotyped, glycoprotein (RG)-deleted, and eGFP-expressing rabies viral particles (RV) were injected into the same region, and mice were sacrificed 5 – 6 days later.

Stereotaxic coordinates for injections:

LC: AP −5.4 mm, ML 0.9 mm, DV 3.7 mm
PB: AP −5.2 mm, ML 1.2 mm, DV 3.2 mm
PPT: AP −4.7 mm, ML 1.2 mm, DV 3.5 mm
TMN: AP −2.5 mm, ML 0.9 mm, DV 5.3 mm
BF: AP 0.1 mm, ML 1.2 mm, DV 5.6 mm
VTA: AP −3.3 mm, ML 0.4 mm, DV 4.3 mm
Posterior CeA: AP −1.6 to −1.7 mm, ML 3.0 mm, DV 4.5 mm
Posterior thalamus: AP −3.3 – −3.4 mm, ML 1.8 mm, DV 3.1 −3.2 mm
PVT: AP −0.4 mm, ML 0 mm, DV 3.6 mm

Optic fibers were implanted into the target region two weeks after viral injection. Electroencephalogram (EEG) and electromyogram (EMG) implants were placed in the same surgery as for optic fibers. To implant EEG and EMG recording electrodes, two stainless steel screws were inserted into the left and right skull 3 mm from midline and 3.5 mm posterior to the bregma (adjusted slightly if an optic fiber is placed near these locations), a reference screw was inserted into the skull on top of the right cerebellum. Two EMG electrodes were inserted into the neck musculature. Insulated leads from the EEG and EMG electrodes were soldered to a pin header, which was secured to the skull using dental cement. Dental cement was applied to cover the exposed skull completely and to secure the implants for EEG and EMG recordings to the screws. After surgery, mice were allowed to recover for 1-2 weeks before experiments.

Polysomnographic recordings

Behavioral experiments were carried out in home cages placed in sound-attenuating boxes between 11:00 am and 6:00 pm (light phase) and between 9 pm and 1 am (dark phase). EEG and EMG electrodes were connected to flexible recording cables via a mini-connector. Recordings started after 20-30 min of habituation. The signals were recorded with a TDT RZ5 amplifier, filtered (1-750 Hz) and digitized at 1,500 Hz. Spectral analysis was carried out using fast Fourier transform (FFT), and the brain state for

each 5 s epoch was classified into NREM, REM and wake states (wake: desynchronized EEG and high EMG activity, NREM: synchronized EEG with high-amplitude, low-frequency (0.5-4 Hz) activity and low EMG activity, REM: high power at theta frequencies (6-9 Hz) and low EMG activity). The classification was made using custom-written MATLAB software.

Sleep deprivation and rebound

Sleep deprivation started at 7 am. Mice were kept awake by introducing novel objects or tapping lightly on the cages. To reduce the possibility of stress, mice were never touched directly. After 6 hr of deprivation, sleep-deprived mice were allowed rebound sleep in their home cages for 2-3 hr before sacrificed.

Optogenetic manipulation

Each optic fiber (200 μm diameter; ThorLabs) was attached through an FC/PC adaptor to a 473-nm blue laser diode (Shanghai laser), and light pulses were generated through the TDT system. Optogenetic activation experiments (in ChR2- or eYFP-expressing mice) were conducted unilaterally, and optogenetic inhibition experiments (in iC++- or eYFP-expressing mice) were conducted bilaterally. Fiber optic cables were connected 20-30 min before the experiments for habituation. Light pulses (10 ms per pulse, 10 Hz, 120 s, 3-6 mW) or constant light (120 s, 3-6 mW) were applied for optogenetic activation and inactivation experiments, respectively. In each optogenetic manipulation experiment, inter-stimulation interval was chosen randomly from a uniform distribution between 7 and 16 min. Each experimental session lasted for 3 h, and each animal was tested for 5-8 sessions. Mice showing no ChR2-eYFP expression in CeA or with misplaced optic fiber (> 500 μm from the NTS neuron cluster) were excluded from behavioral analysis.

Optrode recording

Each optrode consisted of an optic fiber (200 μm in diameter) glued together with 6 pairs of stereotrodes, with two FeNiCr wires (Stablohm 675, California Fine Wire) twisted together and electroplated to an impedance of ~200 kΩ using a custom-built plating device. The optrode was attached to a driver to allow vertical movement of the optrode assembly. Wires to record cortical EEG and EMG from neck musculatures were also attached for simultaneous recordings. A TDT RZ5 amplifier was used for all the recordings, signals were filtered (0.3-8 kHz) and digitized at 25 kHz.

Spikes were sorted offline based on the waveform energy and the first three principal components of the spike waveform on each stereotrode channel. Single units were identified automatically using the software KlustaKwik (http://klustakwik.sourceforge.net). The quality of each unit was assessed by the presence of a refractory period and quantified using isolation distance and L-ratio. Units with an isolation distance < 20 and L-ratio > 0.1 were discarded.

To identify ChR2-tagged neurons, laser pulse trains (15 and 30 Hz with duration of 1 and 0.5 s, respectively) were delivered every minute. A unit was identified as ChR2 expressing if spikes were evoked by laser pulses with high reliability (> 50% for all units in our sample), short first-spike latency (< 7 ms for 22/23 units, 9 ms for 1 unit), low jitter (< 3 ms for all units in our sample), and the waveforms of the laser-evoked and spontaneous spikes were highly similar (correlation coefficient > 97%). To calculate the average firing rate of each unit in each brain state, spikes during the laser pulse trains were excluded.

Immunohistochemistry and immunocytochemistry

For immunohistochemistry, mice were deeply anesthetized and transcardially perfused using PBS followed by 4% paraformaldehyde in PBS. Brains were post-fixed in 4% paraformaldehyde for 24 - 48 h and stored in 30% sucrose in PBS solution for 48 h for cryoprotection. Brains were embedded and mounted with Tissue-Tek OCT compound (Sakura finetek) and 40 μm sections were cut using a cryostat (Leica). For c-Fos induction, light pulses (10 ms per pulse, 10 Hz, 120 s, 3-6 mW, 2 min interval) were given for 0.5 h before sacrificing the animal. For c-Fos staining, brain slices were washed using PBS and subjected to heat-induced antigen retrieval with 0.1 M citric acid (pH 6.0) at 95°C for 5 min. Slices were then washed with PBS, permeabilized using PBST (0.3% Triton X-100 in PBS) for 30 min and incubated with blocking solution (5% normal goat serum or normal donkey serum in PBST) for 1 h followed by primary antibody incubation overnight at 4 °C. The following primary antibodies were used: rat anti-mCherry (1:1000, M11217, Thermo Fisher Scientific) and rabbit anti-c-Fos (1:5000, 226003, Synaptic System). The next day, after sufficient washing in PBS, sections were incubated in proper fluorescently conjugated secondary antibodies (1:500, Invitrogen or Jackson Immuno Research) for 2 h at room temperature. Finally, sections were counterstained with 4',6-diamidino-2-phenylindole dihydrochloride (DAPI; Sigma-Aldrich) and mounted on slides with VECTASHIELD Antifade Mounting Medium (Vector Laboratories, H-1000). Fluorescence images were taken with a confocal microscope (LSM 710 AxioObserver Inverted 34-Channel Confocal, Zeiss), a fluorescence microscope (Keyence BZX-710), and Nanozoomer (Hamamatsu).

For NTS staining, Alexa Fluor 488 Tyramide SuperBoost Kit (B40922, Thermo Fisher Scientific) was used. Briefly, floating brain slices were treated with 3% hydrogen peroxide solution for 15 min to quench the endogenous peroxidase activity and then subjected to heat-induced antigen retrieval as described above. After wash with PBS, slices were incubated in blocking buffer for 1 h. Rat anti-mCherry antibodies together with rabbit anti-NTS (1:5000, 20072, Immuno Star) were applied for at least 18 h at 4°C. Afterward, sections were washed three times with PBS, 10 min each. Poly-HRP-conjugated goat anti-rabbit secondary antibody was applied together with Alexa Fluor 594 goat anti-rat IgG to the slices for 2 h at room temperature. Slices were washed with PBS three times, 10 min each. Tyramide working solution was prepared according to the manufacturer's instructions, and colors were developed with Alexa Fluor 488 Tyramide for 10 min. Reaction stop reagent was applied, and slices were counterstained with DAPI and mounted with

antifade mounting medium. Images were taken with LSM 710 confocal microscope. Cell counting was done with custom-written MATLAB software. Only cells with clear NTS signal were considered as positive. Control group and NTS knockdown group were stained, imaged, and counted in parallel to maximize accuracy of comparison between them.

For immunocytochemistry, 72 h after transfection, cells seeded on PDL-coated (100 μg/mL) coverslips were quickly washed with PBS, fixed with 4% PFA for 20 min, followed by washes with PBS three times, 5 min each. Cells were then incubated in PBS supplemented with 5% normal goat serum and 0.25% Triton X-100 (blocking solution) for 1 h before incubated in primary antibodies (mouse anti-FLAG, 1:1000, Sigma) diluted in blocking solution at 4°C overnight. Samples were washed thoroughly, incubated in Alexa Fluor 488 goat anti-mouse antibodies (1: 500, Invitrogen or Jackson Immuno Research) for 1 h at room temperature. For counterstain of the nuclei, samples were incubated in 1 μg/mL DAPI for 10 min before being mounted on slides with VECTASHIELD Antifade Mounting Medium. Fluorescence images were taken using LSM 710 confocal microscope. FLAG fluorescence intensity was measured with ImageJ software.

Fluorescence *in situ* hybridization (FISH)

FISH was performed with two methods. First, for double staining of *Nts* and *Tac2*, *Nts* and *Pdyn*, *Nts* and *Gad1*, *Nts* and *Slc17a6*, *Nts* and *Cre*, *Nts* and *Fos*, *Nts and Gbx2, NTS and Tcf7l2, Nts* and RV-eGFP for PB and VTA tracing, as well as *Nts* and RV-eGFP in PVT, double FISH was performed using RNAscope assays according to the manufacturer's instructions (Advanced cell Diagnostics). Second, for double staining of *Gad1/2* and RV-eGFP, *Slc17a6* and RV-eGFP, *Prkcd* and RV-eGFP, *Penk* and RV-eGFP as well as *Nts* and RV-eGFP in the posterior thalamic region, FISH-IHC procedure was used. The following primer sequences were used for cloning of *Gad1*, *Gad2*, *Slc17a6*, *Nts*, *Prkcd*, and *Penk* probes (5′ > 3′) (see also Table S1):

Gad1 (sense/anti-sense):
TGTGCCCAAACTGGTCCT / TGGCCGATGATTCTGGTT;
Gad2 (sense/anti-sense):
TCTTTTCTCCTGGTGGCG / TTGAGAGGCGGCTCATTC;
Slc17a6 (sense/anti-sense):
CCAAATCTTACGGTGCTACCTC / TAGCCATCTTTCCTGTTCCACT;
Nts (sense/anti-sense):
ATGAGAGGAATGAATCTCCAGC / TCAGTAGTAGTAGGAACCCCTCT;
Prkcd (sense/anti-sense):
TTCCTGCGCATCTCCTTC / TGCATTGCCTGCATTTGT;
Penk (sense/anti-sense):
CCTGAGGCTTTGCACCTGG / TCCCAGTAGCTCTTTCAGCAG;

To make FISH probes, DNA fragments were amplified using PCR from mouse whole brain cDNA (Zyagen). A T3 RNA polymerase recognition site was added to the 3′ end of the PCR product. The PCR product was purified using a PCR purification kit (QIAGEN). 1 μg of DNA was used for *in vitro* transcription by using digoxigenin (DIG) RNA labeling mix (Roche) and T3 RNA polymerase. After DNase I treatment for 30 min at 37°C, the RNA probe was purified using probeQuant G-50 Columns (GE Healthcare). 50 μm sections were floated off the slide into 24-well plate, treated with 2% hydrogen peroxide for 15 min, fixed for 15 min in 4% paraformaldehyde in PBS at room temperature, pretreated with proteinase K (10 μg/ml) in 10 mM Tris-Cl, pH 7.4, 1 mM EDTA buffer for 15 min at 37°C, fixed again with 4% paraformaldehyde in PBS for 10 min and rinsed with PBS. The sections were incubated with 0.25% acetic anhydride in 0.1 M triethanolamine, pH 8.0, for 15 min and washed with PBS. Pretreated sections were then incubated for 16-20 h at 53-58°C, in a hybridization buffer (50% formamide, 10mM Tris-Cl pH 8.0, 200 μg/ml tRNA, 10% Dextran Sulfate, 1x Denhalt's solution, 600mM NaCl, 0.25% SDS) containing antisense riboprobes. After hybridization, the sections were washed, first with 2 × SSC-50% formamide, then with 2 × SSC, for 15 min at 58-63°C, treated with RNase A (10 μg/ml) for 30 min at 37°C, and finally washed with 2x SSC and 0.2 × SSC twice each for 15 min at 37°C. After blocking for 1hr with 5% normal goat serum in PBS with 0.1% Triton X-100 (PBT), sections were incubated with alkaline phosphatase-conjugated anti-DIG antibody (1:1000, 11093274910, Roche Applied Science) and chicken anti-GFP antibodies (1:500, GFP-1020, Aves Labs) overnight at 4°C. After washing with PBT three times for 20 min, sections were incubated with Alexa Fluor 488 conjugated donkey anti-chicken antibodies (Jackson Immuno Research) for an additional 2h, and washed with PBS three times for 10 min. Probe positive cells were then detected by Fast Red TR/Naphthol AS-MX Tablets (F4523, Sigma-Aldrich). Finally, the sections were treated with PBS containing DAPI and mounted with cover glass.

Translating ribosome affinity purification (TRAP)

TRAP experiment was performed as previously described (Heiman et al., 2014; Nectow et al., 2015). Briefly, mice were sacrificed and the CeA was rapidly dissected on ice with a dissection buffer (1xHBSS, 2.5 mM HEPES [pH 7.4], 4 mM $NaHCO_3$, 35mM Glucose, 100 μg/ml Cycloheximide). Tissues from 4-5 mice were then pooled, homogenized in the homogenization buffer (20 mM HEPES [pH 7.4], 150 mM KCl, 10 mM $MgCl_2$, 0.5 mM DTT, 80 U/ml RNasin, 40 U/ml Superasin, 100 μg/ml cycloheximide and protease). Homogenates were transferred to a microcentrifuge tube and clarified at 2,000xg for 10 min at 4°C. The supernatant was transferred

to a new tube, and 1/9 sample volume of 10% NP40 and 1/9 sample volume of 1,2-diheptanoyl-*sn*-glycero-3-phosphocholine (DHPC, 300mM) were added to the supernatant. This solution was mixed and then clarified at 20,000xg for 10 min at 4°C. The resulting supernatant was transferred to a new tube. This supernatant served as the input. A small amount (50 μl) was taken and added to a new tube containing 100 μL of lysis buffer from Absolutely RNA Nanoprep kit (Agilent) for future input RNA purification. The rest of the supernatant were used for immunoprecipitation with FLAG and HA antibodies.

Immunoprecipitation was performed with an anti-FLAG (F1804, Sigma) and anti-HA (#3724, Cell Signaling Technology) antibody loaded ProteinA Dynabeads (10002D, Thermo Fisher Scientific). The samples and beads were incubated for 1h at 4°C. The beads were washed four times using 0.35M KCl Wash buffer (20 mM HEPES [pH 7.4], 350 mM KCl, 10 mM $MgCl_2$, 0.5 mM DTT, 1% NP40, 40 U/ml RNasin, and 100 μg/ml cycloheximide). After the final wash the RNA was eluted by addition of lysis buffer (100 μL) to the beads. Beads were removed with a magnet. Both the input and IP RNAs are purified with Absolutely RNA Nanoprep kit (Agilent) and analyzed with an Agilent 2100 Bioanalyzer. cDNAs were generated and amplified with SMART-Seq v4 Ultra Low Input RNA Kit. cDNA libraries for RNA-seq were prepared with Illumina Nextera Library Prep Kit and analyzed on an Illumina HiSeq 4000. RNA-seq data were analyzed with RSEM (RNA-Seq by Expectation-Maximization) (Li and Dewey, 2011). Further gene expression analysis was done with DESeq2 software. Transcripts with TPM ((Transcripts Per Kilobase Million) > 1 were used for analysis.

CRISPR/Cas9-mediated gene knockdown

For Cas9 target selection, the 20-nt target sequence was selected to precede a 5′-NGG protospacer-adjacent motif (PAM) sequence. Sequences of *Nts* exon 3, *Slc32a1* exon 2, and *Slc17a6* exon 2 (~200 bp) were submitted to the CRISPR design tool (http://zlab.bio/guide-design-resources) for the selection of sgRNA sequences. sgRNAs with quality score ≧ 95 were chosen. Control sgRNA was designed to target the *lacZ* gene from *E. Coli* (Sequence adopted from Addgene plasmid #60228). Guide oligos were synthesized by IDT (Integrated DNA Technologies), and annealed as described in the CRISPR-Cas9 Mouse Toolbox (https://www.addgene.org/crispr/zhang/). AAV-U6-sgRNA(backbone)-pCBh-Cre-WPRE-hGHpA construct was obtained from Addgene (#60229), and modified by replacing Cre with a DIO-ChR2-mcherry cassette. sgRNAs were cloned to the modified construct according to the CRISPR-Cas9 mouse Toolbox. AAV2 viruses were packaged according to previously described procedures (Hauswirth et al., 2000).

For *in vitro* efficiency test, NTS-FLAG, VGAT-FLAG, and VGLUT2-FLAG expressing plasmid were obtained from OriGene Technologies (MR226576, MR208431, MR209115). Cas9-expressing 368T1 mouse cell line was generous gift from Lin He (UC Berkeley). 1 × 10^5 368T1 cells were seeded on PDL-coated (100 μg/ml) coverslips in each well of 12-well plate in DMEM supplemented with 10% Fetal Bovine Serum (FBS). 24 h later, pU6-sgRNA(backbone)-pCBh-Cre-WPRE-hGHpA, pCMV6-NTS-FLAG or pCMV6-VGAT-FLAG or pCMV6-VGLUT2-FLAG, and *Nts*-targeting, *Slc32a1*-targeting, *Slc17a6*-targeting or *lacZ*-targeting sgRNA expressing plasmids (1 μg of each plasmid for every well) were co-transfected into Cas9-expressiong 368T1 cells with Lipofectamine 2000 Transfection Reagent according to manufacturer's instructions. 72 h after transfection, cells were fixed and stained with FLAG antibodies as described above.

Slice recording

AAV DJ-EF1α-DIO-ChR2-eYFP or AAV DJ-U6-sgRNA (targeting *lacZ* or *Nts*)-pCbh-DIO-ChR2-mCherry (0.3 μl) was injected into the CeA of Nts^{Cre} or Nts^{Cre};*Rosa26-floxed-STOP-Cas9* mice. Acute slices were made 2 weeks after injection. The animal was deeply anaesthetized with 5% isoflurane. After decapitation, the brain was dissected rapidly and placed in ice-cold oxygenated HEPES buffered artificial cerebrospinal fluid (ACSF; in mM: 92 NaCl, 2.5 KCl, 1.2 NaH_2PO_4, 30 $NaHCO_3$, 20 HEPES, 25 glucose, 5 sodium ascorbate, 2 thiourea, 3 sodium pyruvate, 10 $MgSO_4$, 0.5 $CaCl_2$, and 12 NAC, at pH 7.4, adjusted with 10 M NaOH), and coronal sections of the LC, PB, or VTA were made with a vibratome (Leica). Slices (250 μm thick) were recovered in oxygenated NMDG (N-Methyl-D-glucamine)-HEPES solution (in mM: 93 NMDG, 2.5 KCl, 1.2 NaH_2PO_4, 30 $NaHCO_3$, 20 HEPES, 25 glucose, 5 sodium ascorbate, 2 thiourea, 3 sodium pyruvate, 10 $MgSO_4$, 0.5 $CaCl_2$ and 12 NAC, at pH 7.4, adjusted with HCl) at 32°C for 10 min and then maintained in an incubation chamber with oxygenated standard ACSF (in mM: 125 NaCl, 3 KCl, 2 $CaCl_2$, 2 $MgSO_4$, 1.25 NaH_2PO_4, 1.3 sodium ascorbate, 0.6 sodium pyruvate, 26 $NaHCO_3$, 10 glucose and 10 NAC, at pH 7.4, adjusted by 10 M NaOH) at 25°C for at least 1 h before recording. All chemicals were from Sigma.

Whole-cell recordings were made at 30 °C in oxygenated solution (in mM: 125 NaCl, 4 KCl, 2 $CaCl_2$, 1 $MgSO_4$, 1.25 NaH_2PO_4, 1.3 sodium ascorbate, 0.6 sodium pyruvate, 26 $NaHCO_3$ and 10 glucose, at pH 7.4). Inhibitory postsynaptic currents (IPSCs) were recorded using a cesium-based internal solution (in mM: 136 $CsMeSO_4$, 7 CsCl, 10 HEPES, 0.5 EGTA, 4 $MgCl_2$, 4 Na_2ATP, 0.4 NaGTP, 5 QX-314, at pH 7.3, adjusted with CsOH, 290–300 mOsm). Light-evoked responses of ChR2-expressing CeA neurons were recorded with a potassium-based internal solution (in mM: 135 potassium gluconate, 5 KCl, 10 HEPES, 0.3 EGTA, 4 MgATP, 0.3 NaGTP, and 10 sodium phosphocreatine, at pH 7.3, 290-300 mOsm). The resistance of the patch pipette was 3-5 MΩ. The cells were excluded if the series resistance exceeded 40 MΩ or varied by more than 20% during the recording period. To activate ChR2, we used a mercury arc lamp (Olympus) coupled to the epifluorescence light path and bandpass filtered at 450-490 nm (Semrock), gated by an electromagnetic shutter (Uniblitz). A blue light pulse (5 - 10 ms) was delivered through a 40 × 0.8 numerical aperture water immersion lens (Olympus) at a power of 1-2 mW. Data were recorded with a Multiclamp 700B amplifier (Axon instruments) filtered at 2 kHz and digitized with a Digidata 1440A (Axon instruments) at 4 kHz. Recordings were analyzed using Clampfit (Axon instruments).

Single-cell RT-PCR

At the end of each recording, cytoplasm was aspirated into the patch pipette, expelled into a PCR tube as described previously (Chung et al., 2017; Xu et al., 2015). The single cell RT-PCR protocol was designed to detect the presence of mRNAs coding *Slc17a6*, *Gad2*, *Th*, *Gapdh*. First, a cDNA library of the transcriptome of the single cell was generated using the SuperScript III kit (Invitrogen, 18080-051) according to the manufacturer's protocol. Second, multiplex PCR amplification was performed with gene-specific multiplex primer using Accuprime Taq polymerase (12339-024, Invitrogen). Finally, nested PCR was performed using GoTaq Green Master Mix (M7122, Promega) with nested primers for each gene. Amplification products were visualized via electrophoresis using 1.2% agarose gel.

Primers (5′ > 3′) for single-cell RT–PCR were as follows (see also Table S2).

Gapdh (sense/anti-sense):
Multiplex (572bp), ACTCCACTCACGGCAAATTC / CACATTGGGGGTAG GAACAC;
Nested (331 bp), AGCTTGTCATCAACGGGAAG / GTCATGAGCCCTTC CACAAT;
Gad2 (sense/anti-sense):
Multiplex (531 bp), CAGCCTTAGGGATTGGAACA / ACCCAGTAGTCCCCTTTGCT;
Nested (266 bp), GTTCCTTTCCTGGTGAGTGC / TGCATCAGTCCCTCCTCTCT;
Slc17a6 (sense/anti-sense):
Multiplex (662 bp), GCCGCTACATCATAGCCATC / GCTCTCTCCAATGCTCTCCTC;
Nested (506 bp), ACATGGTCAACAACAGCACTATC / ATAAGACACCAGAAGCCAGAACA;
Th (sense/anti-sense):
Multiplex (692 bp), GCCGTCTCAGAGCAGGATAC / TGGGTAGCATAGAGGCCCTT;
Nested (179 bp), GTCTCAGAGCAGGATACCAAGC / CTCTCCTCGAATACCACAGCC;

QUANTIFICATION AND STATISTICAL ANALYSIS

Statistical analysis was performed using MATLAB and GraphPad. All statistical tests were two-sided. The 95% confidence intervals (CI) for brain state probabilities and transition probabilities were calculated using a bootstrap procedure: For an experimental group of n mice, with mouse i comprising m_i trials, we repeatedly resampled the data by randomly drawing for each mouse m_i trials (random sampling with replacement). For each of the 10,000 iterations, we recalculated the mean probabilities for each brain state and each transition across the n mice. The lower and upper confidence intervals were then extracted from the distribution of the resampled mean values. To test whether a given brain state or state transition is significantly modulated by laser stimulation, we calculated for each bootstrap iteration the difference between the mean probabilities during laser stimulation and the preceding period of identical duration (combining all time bins within each period). The p value was determined from the distribution of the differences in 10,000 iterations. To compare the degree of laser-induced brain state changes between two groups of animals, in each iteration we resampled the data for each group separately. The laser effect (difference between the pre-laser and laser periods) was computed for each group, and the difference between the two groups was computed. The p value was determined from the distribution of the differences in 10,000 iterations.

DATA AND SOFTWARE AVAILABILITY

Processed and raw data of TRAP RNA-seq have been deposited in the Gene Expression Omnibus under accession number GEO: GSE121888.